Title
ELASTIC K+ -PROTON SCATTERING AT 910 MeV/c POLARIZATION OF THE RECOIL PROTONS

Author
Hirsch, Warner.

Publication Date
1963-05-01

University of California

Ernest O. Lawrence Radiation Laboratory

ELASTIC K^+-PROTON SCATTERING AT 910 MeV/c. POLARIZATION OF THE RECOIL PROTONS

Berkeley, California

DISCLAIMER

Research and Development

UCRL-10813
UC-34 Physics
TID-4500 (19th Ed.)

UNIVERSITY OF CALIFORNIA

Lawrence Radiation Laboratory
Berkeley, California

Contract No. W-7405-eng-48

ELASTIC K^+-PROTON SCATTERING AT 910 MeV/c. POLARIZATION OF THE RECOIL PROTONS

Warner Hirsch

(Ph. D. Thesis)

May 1963

Printed in USA. Price $2.25. Available from the
Office of Technical Services
U. S. Department of Commerce
Washington 25, D.C.

Contents

ELASTIC K^+-PROTON SCATTERING AT 910 MeV/c. POLARIZATION OF THE RECOIL PROTONS

Warner Hirsch

Lawrence Radiation Laboratory
University of California
Berkeley, California

ABSTRACT

The Berkeley 30-in. propane bubble chamber was used to study the elastic K^+-proton interaction at 910 MeV/c, in the region of transition from the isotropy in angular distribution found below 810 MeV/c to the rapidly increasing anisotropy above 1 BeV/c.

Results based on 1154 events show that the series $(1 + a \cos \theta_k^{cm})$ can fit the angular distribution with $a = 0.18 \pm 0.05$.

Polarization was measured on the secondary proton by using proton-proton and proton-carbon recoils in the liquid of the chamber.

A likelihood function using 53 proton-proton and 41 proton-carbon interactions gave these values for the polarization:

$$\begin{cases} \bar{P}\ (40^\circ \leq \theta_k^{cm} < 70^\circ) = -0.80 \pm 0.80 \\ \bar{P}\ (70^\circ \leq \theta_k^{cm} < 100^\circ) = -0.74 \pm 0.45 \\ \bar{P}(100^\circ \leq \theta_k^{cm} < 140^\circ) = +0.55 \pm 0.93 \\ \bar{P}(140^\circ \leq \theta_k^{cm} < 160^\circ) = +0.70 \pm 0.93 \end{cases}$$

The results of a phase shift analysis incorporating these polarization data are presented.

INTRODUCTION

The purpose of this experiment is to investigate K^+-proton elastic scattering in an intermediate energy region, between the isotropy that seems to characterize the angular distribution below 810 MeV/c[1,2,3] and the rapidly increasing anisotropy found to exist above 1 BeV/c[4,5].

The work of Goldhaber et al.[1] indicates that the very low energy K^+ - P interaction is characterized by an isotropic angular distribution, by constructive interference between nuclear and Coulomb interactions (therefore by a repulsive nuclear force), and by an S-wave phase shift the magnitude of which increases linearly with momentum at least as far as the 640 MeV/c region. A description of the scattering in terms of a $P_{1/2}$ interaction, or a mixture of $P_{1/2}$ and $P_{3/2}$ states, which can also reproduce isotropy, is ruled out by them on the basis of the low energy behavior and the constant character of the angular distribution over this whole momentum region. These results are not in disagreement with the earlier work of Kycia, Kerth and Baender[2]. At 810 MeV/c isotropy is still a possible description of the observed angular distribution.[3]

The results of Cook et al.[4,5] at 970, 1170, and 1970 MeV/c show that some anisotropy appears definite at around 1 BeV/c, increasing rapidly in importance. Their 1970 MeV/c data is interpreted with an optical model approach because most of the angular distribution here looks like predominantly a diffraction interaction.

Our present experiment is to measure the angular distribution in the region of transition, at 910 MeV/c, to try to determine, with the aid of polarization measurements on the recoil proton, the nature

of the angular momentum states involved in the interaction. If good polarization data are available, it is, in principle, possible to distinguish between pure angular momentum states and mixtures.

Since proton-carbon scatters have high analyzing power, it was advantageous to conduct the experiment in propane (C_3H_8).

The experimental arrangement[6] shown in Fig. 1 was used to lead 910 MeV/c K^+ mesons from the Bevatron target to the Powell-Birge 30-in. propane bubble chamber[7] with which 42,500 pictures were taken. A scan of 19,750 pictures for two-prong scatters yielded 4982 candidate events of the type shown in Fig. 2. These were measured on digitized microscopes and constrained in energy and momentum to be elastic K^+ - Proton interactions.

Of the 4982 events, 1905 had readily identifiable scattered prongs, in that a) the proton came to rest in the liquid of the bubble chamber, or b) the K^+ decayed after scattering, or c) the K^+ went in a backward direction with respect to the incoming beam particle. For other events a scan table comparison of predicted and observed ionization density and δ-ray formation gave the correct identity of the scattered prongs.

1154 events were included in the angular distribution after constraint to elastic K^+ - Proton scattering (See Fig. 3).

To obtain maximum effectiveness from phase shift fitting, the polarization of the recoil proton was measured by second scattering in the liquid of the bubble chamber.

For this purpose all 42,000 pictures were scanned for good K^+ - P elastic scatters that were followed by interactions of the recoil protons either on hydrogen or on carbon (Fig. 4). Good P-hydrogen events had to be coplanar and have 90° opening angle between the scattered protons. Good P-carbon events had to lie in the acceptable

region of a modified Fowler-Birge[8*] plot and to show no evidence for an energy loss greater than 50 MeV.

There were 94 events that met all these criteria (41 P-carbon and 53 P-hydrogen events).

The polarization information was used, with the measured angular distribution, to obtain the best sets of phase shifts to describe K^+ - Proton elastic scattering (Table I and Fig. 5).

The following equations, which are discussed in detail in appendices A and B, were used to analyze our data.

(1) The angular distribution is given by:

$$\frac{d\sigma}{d\Omega} = |g|^2 + |h|^2, \text{ where}$$

$$g = \frac{\sqrt{4\pi}}{2ik} \sum_{L=0}^{\infty} \sqrt{\frac{1}{2L+1}} \left[(L+1) A_{L,\, L+1/2} + L A_{L,\, L-1/2} \right] Y_L^0(\theta)$$

$$h = \frac{\sqrt{4\pi}}{2ik} \sum_{L=0}^{\infty} \sqrt{\frac{L(L+1)}{2L+1}} \left[A_{L,\, L+1/2} - A_{L,\, L-1/2} \right] Y_L^1(\theta)$$

where θ is the scattering angle; L is the angular momentum; k is proportional to the incoming momentum; and where we have set

$$A_{L,J} = e^{2i\delta_{L,J}} - 1$$

Coulomb scattering causes a modification of these equations, as is shown in the references 4, 5, and 16. This has been taken into account in the experiment.

(2) The polarization of the recoil proton at the first scatter is

$$P_o(\theta) = \frac{2 \operatorname{Re} g h^*}{|g|^2 + |h|^2}$$

and is directed along the normal to the first scattering plane.

(3) The differential cross-section for protons at the second scatter is

$$\frac{d\sigma}{d\Omega} \propto (1 + P_o P_1 \cos \Phi)$$

where P_1 is the analyzing power at the second scatter and Φ is the angle between the first and second scattering planes.

* The data in this reference, as greatly expanded by V.Z. Peterson, describe elastic P-Carbon interactions and degrees of inelasticity of P-carbon interactions up to a proton energy loss of 50 MeV.

EXPERIMENTAL PRODEDURE

I. Apparatus

The beam transport equipment, designed by Goldhaber, et al.[6], provided a momentum-analyzed and velocity-separated beam of K^+ (Fig 1). Protons impinged on a target in one of the Bevatron straight sections. Particles travelling at 27.5° to the circulating proton beam were allowed to enter the beam transport channel after passing through a collimator to reduce the vertical size of the image. Momentum analysis took place at a bending magnet and momentum selection in a horizontal collimator behind the magnet. This collimator and the focussing properties of the fringing field of the bending magnet created a parallel beam which was passed through a ten-foot, crossed-field velocity spectrometer to cause a vertical displacement of π^+ and K^+ images. These were focussed by a two-element quadrupole magnet on a slit which was so placed as to admit preferentially K^+. The rest of the beam was a mirror image of what has been described so far, forming a final image at a second slit. Behind this was placed the 30-in. propane bubble chamber. Extra maneuverability was obtained by a small C magnet in front of the first slit. A horizontal collimator was placed within the first quadrupole magnet to keep the beam off the walls of the second velocity spectrometer.

"Separation curves" (Fig. 6) were run by tuning both spectrometers for K^+, then varying the magnetic field in one to sweep over a broad region around the best K^+ operating point.

The Powell-Birge 30-in. heavy liquid bubble chamber[7] was filled with propane (C_3H_8; density = 0.415 grams/cc) and placed in a 13,000 gauss magnetic field. It was equipped with two cameras horizontally

separated by 22.9 cm and situated 140 cm above the propane vessel itself.

The tracks were measured by making (X,Y) coordinate observations with digitized microscopes in both stereo views at intermittent points along the track length. Computation consisted of spacial reconstruction of tracks, evaluation of momenta, angles, and error estimates, calculation of derived quantities (i.e. energies, center of mass values of the parameters, etc), and constraint of all measured quantities to fit the hypothesis of elastic K^+ - P scattering. All these functions were performed by the FOG-CLOUDY-FAIR data reduction system[9].

II. Scanning

Scanning instructions specified:

a) that an event have two and only two outgoing prongs;

b) that the incident K^+ enter the bubble chamber within 10^o of the average beam direction, and that it have no other interaction prior to the two-prong scatter;

c) that both scattered prongs not lie to one side of the incident track in both views; that both scattered prongs not go backward with respect to the incident track;

d) that the scattered prongs obey the "scissors test"*;

e) that a track coming to rest in the liquid of the chamber, without decaying, be labelled "proton";

f) that a track whose ionization becomes less dense abruptly, accompanied by a scatter at this point, be labelled "K^+ decay" unless the kinematics violate this hypothesis;

g) that a track scattered backward with respect to the incident track be labelled "K^+", and, finally,

h) that all δ-rays on any prong be noted.

Instruction (a) is intended to eliminate a portion of the inelastic interactions on hydrogen or carbon. Item (b) requires that the beam momentum be up to the average, since tracks scattered on the beam transport equipment or in the propane itself will have a reduced momentum. Items (c) and (d) are rough elasticity and coplanarity tests. Items (e), (f), and (g) take advantage of the known characteristics of K^+'s and protons to help identify the scattered prongs. Item (h) is used for subsequent identification of prongs; using the measured momentum value one can differentiate frequently between K^+ and proton on the basis of δ-ray formation. This is also a method of removing π^+ contamination,

* The "scissors test" is a rough indication of the coplanarity of all three tracks at an origin: one coalesces both images of the beam track on a scanning projector. Then, rapid switching from one projected view to the other will cause the scattered tracks to appear to move back and forth like a pair of scissors if the event is coplanar. If, however, one prong goes backward with respect to the beam particle then the track images will appear to move in the same direction rather than in opposite directions for coplanar tracks. Either criterion could be obeyed.

since the K^+ cannot make δ-rays of greater energy than 5 MeV.

Tracks less than 3 mm in length were rejected.

Out of 19,750 pictures scanned with these instructions, 4982 candidates for K^+ - Proton elastic scattering were observed and measured.

For the second portion of this experiment, the measurement of the recoil proton polarization, an instruction was given to note all interactions on scattered prongs. Another 22,750 pictures were scanned only for such second scatters. The whole film yielded 1757 of these events.

The final angular distribution contains events only from the fully scanned 19,750 picture sample, whereas the polarization measurements use all the available film. The fully scanned rolls of film are interspersed within the total footage to ensure proper sampling.

Of the 4982 candidate events for the angular distribution, 1905 fell under scanning instructions (e), (f), and (g) and thus had their scattered prongs identified. The remaining 3077 events had to be constrained to two elasticity hypotheses corresponding to the possible identity permutation of the scattered tracks ($[K^+, P]$ and $[P, K^+]$).

III. Selection Criteria

A. Elasticity Criteria

Elastic scattering experiments on hydrogen in a propane chamber are characterized by high background since only one third of the possible interactions take place on free protons. We have three momentum and one energy conservation conditions on nine measured variables (one momentum and two angles define each track). Using the method of Lagrange undetermined multipliers as it is described in Berge, Solmitz and Taft,[10] a best fit to the elasticity hypothesis and a χ^2 goodness of fit estimate are obtained.

We chose a χ^2 cut off of 10* ($P\left[\chi^2\right] = 0.04$; Fig. 7).

Two tests were made to show that this cut off was justifiable. Fig. 8 shows the distribution of "quasi-elastic" events, defined as those which had $10 < \chi^2 < 40$ and also fulfilled the conservation equations after constraint. These are interactions with peripheral protons in carbon. Comparison with the elastic distribution shows that, within statistics, both have the same angular distribution. Thus, choosing our cut off at $\chi^2 = 10$ does not introduce a bias in the angular distribution.

Fig. 9 shows a plot of the Q value of the scattered prongs (where $Q \equiv \left[\left(\sum_i E_i\right)^2 - \left(\sum_i \vec{P}_i\right)^2 \right]^{1/2} - \sum_i M_i$) for events with $\chi^2 > 10$. These are overwhelmingly carbon events, although a few inelastic and

---

* The measured χ^2 distribution in bubble chamber data is often found to be of correct shape but displaced too far toward higher values of χ^2. This is due to a general underestimation of measurement errors, and must be corrected before a cut off limit can be meaningful. Our errors were underestimated by a factor of 1.22.

elastic K^+ - P interactions are included. The histogram shows what may be called the "carbon phase space." From an experiment of $K^+ + n \rightarrow K^o + P$, conducted at 770 MeV/c in propane, we have a Q value distribution of the two outgoing prongs. This distribution, normalized to our data and shown in a solid line in Fig. 9, is from an interaction which must have taken place in carbon. It provides a test to see whether the rejected events with $\chi^2 > 10$ really are carbon scatters. As is seen, our histogram fits a "carbon phase space" very well, except for an enhancement in the region of 300 MeV. This is due to those 4% (or about 60 events) of elastic scatters with $\chi^2 > 10$, which lie in the tail of the χ^2 distribution.

Having chosen our χ^2 cut off, we then went back to the scan table and looked at those events with $\chi^2 < 10$ where scattered prongs had not previously been identified. Using the computed momentum from curvature, and compensating for the dip angles of the tracks, we compared predicted and observed ionization densities to differentiate between the scattered K^+ from the proton.

Whenever possible we used the δ-rays to aid us. δ-ray formation is a function of velocity and therefore a K^+ of given momentum will form more than a proton of the same momentum. The maximum energy of a δ-ray also is velocity dependent. For momenta below 600 Mev/c, for example, a proton will not create δ-rays of sufficient energy to be visible in propane.* At 910 MeV/c protons can give δ-rays of 0.97

---

* This minimum δ-ray energy is approximately 0.4 MeV, though straggling may cause variation in this. In propane an electron of energy greater than 1.0 MeV will lose 1 MeV per centimeter.

MeV whereas K^+ can produce δ-rays of up to 3.5 MeV.

In some cases it was possible to use range-curvature to pick out the K^+.

π^+ - Proton background interactions can also frequently be detected by using these methods.

By using these three techniques (ionization, δ-rays, and range-curvature) we were able to identify 90 to 95% of scattered tracks. The remainder consisted of: 1) those better suited, by observation, to be π^+ than K^+ and 2) those events where tracks were so poor in quality as to be unidentifiable. In the latter class were very steep tracks where ionization density was unreadable, much kinked tracks where momentum or range were unmeasurable*, and lastly, events falling in regions where temperature gradients caused distortions in the media between the cameras and the chamber.

The χ^2 test after constraint of measured variables is meaningful only if the constraints have indeed been satisfied through this adjustment. Thus we required that the energy conservation equation balance to within 5 MeV, that longitudinal and transverse momenta balance to within 5 MeV/c, and that coplanarity balance to within 17 minutes of arc.** Actually, all these quantities should, after constraint, balance exactly; yet, rounding errors and the finite number of computation iterations performed to achieve convergence can cause some apparent imbalance. Just one more iteration might have caused complete convergence, then the imbalance would be a reflection of mathematical rather than physical limitation and the event ought to

---

* Since there are four constraint equations, we can deliberately omit measuring the momentum of a bad track, use a constraint to supply it and still have three conditions left to impose on the event.

** The coplanarity is $\left|(\vec{K}_{incident} \times \vec{P}_{recoil}) \cdot \vec{K}_{scatt.}\right|$ and is required to balance within 0.005 in the cosine of the dot product angle.

be labelled as "good". Out of the 4982 candidate events sent to the computer, 1448 or 29% passed the combined χ^2 and "converged constraints" tests.

B. π^+ contamination

The contamination of π^+ and μ^+ was measured by use of δ-rays. First a special scan was made[11] of film from another experiment with known π flux in the same energy region. A count was made of beam track δ-rays with more than 5 MeV, and -- separately -- of beam track interactions. These δ-rays must come from π or μ, while the interactions must come from π alone. By comparing this with results from our experiment, we concluded that the combined π and μ background was $(8.9 \pm 0.5)\%$, on the basis of 307 δ-rays greater than 5 MeV on 6735 meters of beam track. The π contamination alone is $(5.9 \pm 1.2)\%$ on the basis of 23 δ-rays greater than 5 MeV found on tracks that subsequently interacted.

To ascertain the maximum possible contamination of our final, selected sample of data, we plotted theoretical curves of θ_k, the laboratory scattering angle of the K^+, versus θ_p, and of θ_π versus θ_p, Fig 10a. Good elastic K^+ - P scattering events were placed (before constraint) on this scatter diagram. Their displacements from the (θ_k vs. θ_p) curve and from the (θ_π vs. θ_p) curve were each plotted in histograms shown in Fig. 10b and 10c. Experimental measurement errors in angles are less than 1.0°. (See Fig. 11).

The displaced peak indicates indeed that these events are better fitted to K^+ - P than π^+ - P scattering. Yet there is a region, for small θ_k or θ_π, where the theoretical curves approach each other to an angular separation that is of the order of magnitude of the errors. In this region some overlap is found, and this gives the upper limit to the actual π^+ contamination of our final data.

We have divided the events into those which lie in the region of possible overlap and those which do not. The latter invariably lie at least 1° farther from the (π, p) curve than the (K, p) curve. In other words, π^{+} contamination is rejected in scanning and by the constraint program, and where no overlap should exist, we have found none. Thus the background of π^{+} - P events must exist solely within the overlap region.

If we say that any event, lying in the overlap region and within 1° of the $(\theta_{\pi}$ vs. $\theta_{p})$ curve, could be a π^{+} - p scattering event, and if we further say that the maximum π contamination of any given set of scattering events is given by the $5.9 \pm 1.2\%$ * determined above, then we find a maximum π contamination of our finally selected data of 0.5%. We estimate that this is well within the errors due to statistics.

---

*This assumes that the angular distribution of (π^{+}, p) is similar to that of (K^{+}, P). Actually the (π^{+}, p) distribution is peaked forward more than the (K^{+}, P) at this energy.[24] Compensation for this brings the maximum π^{+} contamination up from 0.5% to 1.0%.

C. Beam Momentum

In Fig. 12 we show a plot of measured beam momentum along with a fitted Gaussian curve. The value 910 ± 70 MeV/c was obtained. A study of τ decays[12] gave a result (also averaged over the length of the chamber) of 910 ± 60 MeV/c. The momentum loss of the K^+ over the length of the bubble chamber gives a minimum momentum spread of ± 50 Mev/c; these errors are not much wider than this.

Frequently, in experiments with well-analyzed beams of particles, one is able to "edit" the measured value of beam momentum; that is, one constrains it to be the value fixed by the magnets and collimators of the beam transport equipment. This was not possible here because the beam was really designed to operate at about 700 MeV/c, and all parameters were strained beyond original intention to achieve the present momentum. All alterations were performed on the equipment as it sat -- aligned -- on the bevatron floor and no extra wire orbits were run on the magnets or quadrupoles. Thus it was impossible to predict, exactly, what the actual momentum in the bubble chamber would be.

The K^+ - P angular distribution is known to vary only slowly with momentum in this region. Nevertheless some cut off limits are necessary. We chose 910 ± 100 MeV/c, about 1.5 standard deviations.

D. Azimuthal Angle

The K^+ - P interaction, assuming a spherically symmetric potential, must be invariant under the rotation of coordinate axes about the incoming (beam) direction. To test this, in Fig. 13 the azimuthal angle, φ, was plotted. It shows a generally isotropic distribution except for regions at 0°, 180°, and 360°. These are the angles of particles heading almost straight up or down in the chamber. These tracks are hard to see and hard to measure, and we are biased against them. To correct for this, we impose the following acceptable regions on the azimuthal angle φ:

$$10^\circ \leq \varphi \leq 165^\circ$$

$$190^\circ \leq \varphi \leq 340^\circ$$

These limits were imposed after a detailed study of Fig. 13 and similar graphs.

E. Other Selection Criteria

There was, in addition, a fiducial region criterion so that all events would lie in easily visible regions of the bubble chamber. This ensured that scanning efficiency would not vary too rapidly with the position of the interaction vertex.

A last criterion specified that the error (after constraint) in θ_k^{cm}, the center of mass scattering angle of the K^+, be small enough to minimize the chance of events overlapping into adjoining angular distribution boxes. This required an error of less than 6^o in θ_k^{cm}. Only four events were affected.

IV. Angular Distribution

In Fig. 3 we show the angular distribution of the 1154 events that met the selection criteria. This was analyzed with a likelihood function to obtain best fits with a varying number of terms in a cosine series.

A plot of the number of degrees of freedom, n, versus Chi-squared divided by n * (Fig. 14) shows that either

$$\frac{d\sigma}{d\Omega} \propto 1 + (0.18 \pm 0.05) \cos \theta_k^{cm} \qquad (1)$$

or

$$\frac{d\sigma}{d\Omega} \propto 1 + (0.20 \pm 0.06) \cos \theta_k^{cm} + (0.18 \pm 0.12) \cos^2 \theta_k^{cm} \qquad (2)$$

will satisfy the angular distribution. The former is more satisfactory because the addition of the $\cos^2 \theta_k^{cm}$ term does not change the coefficient of the $\cos \theta_k^{cm}$ term appreciably; on the other hand, the coefficient of $\cos^2 \theta_k^{cm}$ is subject to a standard deviation almost as large as itself.

---

* The plot of (n) versus $(\chi^2/_n)$ is based on the fact that the average value of χ^2 is n. Thus we expect that a distribution that is well fitted by 3 coefficients will get a very high χ^2 value when fitted with one coefficient, a lower value with 2 coefficients and approximately 1 with 3 or more coefficients.

V. Polarization

From the unknown polarization (P_o) induced in a direction $\hat{n}_1$ at the first vertex, the known analyzing power (P_1) in direction $\hat{n}_2$ at the second vertex and cos Φ, defined as the projection of $\hat{n}_1$ on $\hat{n}_2$, the following likelihood function was constructed:

$$\mathcal{L}(P_o) \propto \prod_i^k (1 + P_o P_{1_i} \cos \Phi_i) \qquad (1)$$

The product is over the k second scattering events to be used in various phases of this analysis. The basis for this likelihood function is that the differential cross-section at the second scattering vertex is

$$\frac{d\sigma'}{d\Omega} \propto (1 + P_o P_1 \cos \Phi),$$

as is proved in Appendix A.

The proportionality sign is used in Eq. (1) above because many factors not depending on P_o have been omitted. These serve only to change the arbitrary scale of the likelihood function, neither affecting its shape nor the location of its maximum when plotted as a function of P_o. Since the likelihood function is a product of probabilities, it actually includes the total probability that, say, the i^{th} event scattered through $(\theta_{1_i}, \varphi_{1_i})$ at vertex 1, survived undeflected to vertex 2, and scattered there through $(\theta_{2_i}, \varphi_{2_i})$.

A set of input values, P_o, then gives a curve with a maximum that defines the most probable value of P_o, averaged over the data under consideration, and a width that defines the uncertainty in this value.

For later combination with a phase shift analysis we have used $\mathcal{L}$ to find a value of $\overline{P}_o$ in four intervals of θ_k^{cm}, the center of mass scattering angle of the K^+.

Selection criteria for the events to be included in this analysis are discussed in the following sections. 94 events were selected: 41 P-carbon and 53 P-hydrogen scatters. They are shown plotted in Fig. 17. The ordinate is to be interpreted as the "equivalent number of events of unit analyzing power"; it is the sum $\sum_i (P_{l_i} \cos \Phi_i)$ for all events falling into the same interval of θ_k^{cm}. This corresponds to counting up the total effective analyzing power in that interval. It might also be thought of as the number of events that an equivalent counter experiment (of such geometry that $\cos \Phi_i = 1$ and $P_{l_i} \approx 1.00$) might have recorded.

In Fig. 17 we have separated the two classes of second scatters, P-carbon and P-hydrogen. It will be noted that the P-carbon events tend to cluster in the region $\theta_k^{cm} < 90^\circ$ (forward scattered K^+ and backward scattered proton) while the P-hydrogen events tend to lie in the other center of mass hemisphere. This means that, in the laboratory P-hydrogen scatters tend to occur to the faster protons, whereas P-carbon scatters tend to be found on the slower protons.

Though the P-P cross section is nearly constant throughout this energy region (70 to 500 MeV), the P-P scatters tend to occur on the faster protons because these lie forward in the chamber and have much longer path lengths with greater likelihood of interaction. P-C scatters, on the other hand, rapidly become inelastic at higher energies. The maximum angle of scattering of elastic events of higher energy shrinks to 10°. Unless such a small scatter is nearly horizontal it may not be visible.

We have fewer P-C events than P-P though the P-C cross section is larger because:

1. There is 8/3 as much hydrogen as carbon in propane.

2. There are more channels for inelastic P-C than for inelastic P-P collisions.

3. P-C scatters tend to be small in angle and hard to detect.

Eq. (1) cannot be used for bubble chamber events without including a geometric correction factor. Since the existence of this factor was first called to our attention by Dr. Malcolm Whatley[13], we shall henceforth refer to it as the Whatley Correction. A detailed explanation is complicated and is left to Appendix D.

For the purposes of this section, we need only point out that since the measurement of polarization is based on an azimuthal asymmetry at the second scattering vertex, we must be able to detect, for given scattering angle, all azimuthal directions. In other words, protons, scattering in a cone of half angle α about the direction of the incident proton, must all be visible. If the second scatter occurs near the top or bottom of the bubble chamber, for some azimuthal directions the protons may leave projected track lengths too short to be seen in the photographs. This forms a bias in polarization measurement. Each event must be corrected individually. 12% of our events were affected.

We now state the results of the application of Eq. (1), as modified by the Whatley correction, to the four intervals of θ_k^{cm} chosen on the basis of the distribution shown in Fig. 17:

$$\bar{P}_o \quad (40^\circ \leq \theta_k^{cm} < 70^\circ) = -0.80 \pm 0.80$$

$$\bar{P}_o \quad (70^\circ \leq \theta_k^{cm} < 100^\circ) = -0.74 \pm 0.45$$

$$\bar{P}_o \quad (100^\circ \leq \theta_k^{cm} < 140^\circ) = +0.55 \pm 0.93$$

$$\bar{P}_o \quad (140^\circ \leq \theta_k^{cm} < 160^\circ) = +0.70 \pm 0.93$$

The corresponding curves, with the logarithm of $\mathcal{L}(P_o)$ plotted versus P_o, are shown in Fig. 18.

VI. Second Scattering Selection Criteria

A. General Remarks

To be useful for polarization measurements, second scatters must fulfill two conditions: a) they must occur on proton recoils from an elastic first scatter, and b) they must be interactions for which polarization measurements have been carried out in some previous experiment.

Condition (a) is necessary so that a well-defined polarization state exists. Condition (b) requires that the analyzing power at the second scatter be known. The analyzing power is equal to the state of polarization that would be induced by such a scatter on an unpolarized beam of protons of the same momentum.

Elastic proton-hydrogen interactions have previously had analyzing power recorded over a large energy region. Proton-carbon scatters have been investigated in the region from perfect elasticity to an energy loss of 50 MeV.[8]

The momentum of the incident proton at the second vertex was well known because this proton had previously been constrained at the first vertex. The momenta of the scattered tracks at the second vertex are often hard to measure because the tracks are steep. The angles of such tracks, however, can still be well-measured.

By convention, the angle of scattering referred to in P-P interactions is the smaller of the two scattering angles, corresponding to the forward hemisphere in the center of mass.

blank page

B. Proton Hydrogen Interactions

Second scatters with two visible outgoing prongs were tested in two ways as being possible elastic P-P scatters.

First, all three tracks were required to be coplanar within certain limits. These cut off points were chosen after inspection of Fig. 15a where the value of the triple product of the momentum vectors has been plotted. This centers at zero (perfect coplanarity).

The second requirement was that the laboratory opening angle of the two outgoing protons be within the limits shown in Fig. 15b. This angle is / nearly constant for a given incoming momentum. The spread shown is due to the spread in this momentum, as well as to measurement error.

Events which met these two tests and which also were good K^+ - P elastic scatters at the first vertex* were given appropriate analyzing power from the graph in the Fowler-Birge paper[8].

---

* Six requirements have been mentioned for inclusion of an event in the angular distribution. Of these, only the elasticity and beam momentum restrictions were kept for polarization candidates. The other requirements deal with scanning and graphing biases which are not applicable to the likelihood function approach used in this analysis.

C. Proton-Carbon Interactions

The first requirement on prospective P-C scatters was that they should be elastic to within 50 MeV. This information was obtained from a (modified) Fowler-Birge plot[8] of incoming proton momentum versus scattering angle.

The curves that yielded the analyzing power were divided into several categories of increasing inelasticity, with decreasing analyzing power. Therefore we next studied the photographs using all available information, such as momentum, dip angle, measurement error, and ionization density to estimate the amount of energy loss.

There were a few recoil protons that came to rest in the chamber. Their momentum was known to 3% and their energy loss could be accurately determined. Other events, if obviously inelastic, also received a lowered analyzing power. In most cases, however, the amount of inelasticity could not be established. Such events were arbitrarily labelled "elastic". This is reasonable because of the very high (300 mb.) cross section for elastic scattering.

If an event fell in a region where the analyzing power had not been measured, or could not be found by a short extrapolation, we did not use it. 41 events were finally used.

A bias is introduced by the fact that some of the P-carbon scatters at small angles are really P-hydrogen scatters with proton recoils too short to be seen in propane. The maximum P-P analyzing power of 45% is only half the maximum P-C analyzing power.

To resolve this bias, we plotted the laboratory angular distribution of P-C and P-P scatters as shown in Fig. 16. The P-P angular distribution (when plotted in terms of cosine) is

isotropic at our energies.[14] We found that portion of our distribution which is indeed a straight line and extended it to a cosine value of 1.0, to estimate the number of missing P-P scatters.

Not all the P-C scatters in the angular region of the extrapolated line could be P-P, since some configurations would have produced visible recoils.

We estimated that there were 9.8 hidden P-P events in 54 elastic and inelastic P-C scatters. Therefore each P-C event, if used for the polarization, was assigned a mixed analyzing power, (82% $\left[\text{P-C}\right]$ + 18% $\left[\text{P-P}\right]$).

D. Cosine Φ Determination

The analyzing power assigned in the preceding sections must be multiplied by the cosine of the angle between the normals to the first and second scattering planes. These normals are defined by the cross products:

$$\vec{n}_1 = \frac{\vec{P}_{Kin} \times \vec{P}_{po_1}}{|\vec{P}_{Kin} \times \vec{P}_{po_1}|} \; ; \; \vec{n}_2 = \frac{\vec{P}_{po_2} \times \vec{P}_{p_{sc}}}{|\vec{P}_{po_2} \times \vec{P}_{p_{sc}}|} \; ; \; \cos \Phi = \vec{n}_1 \cdot \vec{n}_2. \qquad (1)$$

This assumes that neither the proton's velocity nor spin has been disturbed between scatters. $\vec{n}_1$ and $\vec{n}_2$ are defined in terms of the momenta of the incident K^+ $\left[P_{Kin}\right]$, of the recoiled proton at the first scatter $\left[P_{po_1}\right]$, of the incident proton at the second scatter $\left[P_{po_2}\right]$, and of the scattered proton at the second scatter $\left[P_{p_{sc}}\right]$. $\vec{n}_1$ and $\vec{n}_2$ are the orientations along which polarizing and analyzing of the proton spin can occur. Cos Φ gives the projection of $\vec{n}_1$ on $\vec{n}_2$.

Generally P_{po_1} is set equal to P_{po_2} since both quantities refer to the same particle, but we must consider the effects of the magnetic field and of the medium (propane) on the spin orientation of the proton before we can do this.

The magnetic field $\vec{B}$ causes spin precession separately about the direction of $\vec{B}$ and about the velocity direction, $\vec{v}$. The vector $\vec{v}$ itself changes orientation at the cyclotron frequency as the proton moves in the field.

The medium slows down the proton and also may cause some depolarization. The slowing down affects both the spin precession and the rotation of the velocity vector. It also affects the analyzing power since this is momentum dependent.

A detailed discussion of the relative importance of these factors is found in Appendix C. We here only state the results.

The spin precession formula is due to G. W. Ford[15].

$$\vec{\omega}_o = \frac{e\vec{B}}{m\gamma c}\left[1 + \left(\frac{g}{2} - 1\right)\gamma\right] - \frac{\vec{v}}{|\vec{v}|}(\gamma - 1)\left(\frac{g}{2} - 1\right)\left(\left[\frac{eB}{m\gamma c}\right] \cdot \left[\frac{\vec{v}}{|\vec{v}|}\right]\right).$$

We have neglected the second term, the precession component about the velocity, and have thereby introduced an error of at most ± 12% in the precession angle.

There is also at most a ±10% variation in the magnitude of $\vec{B}$ over the bubble chamber, which gives rise to a similar error in the precession angle.

Neglecting the effect of the proton energy loss on the spin precession causes an underestimation of precession angle by at most 12%.

Depolarization of protons does occur to some extent[14] but no complete information covering a wide range of energies and angles is available. (Triple scattering experiments are needed to give this information.) We have not included this correction, and have therefore underestimated the polarization by some unknown factor.

The rotation of $\vec{v}$ between first and second scatters is compensated by a rotation of the coordinate system at the second scatter about the field direction.

The analyzing power is adjusted to the calculated momentum loss.

All neglected known corrections can add to give a 34% uncertainty in the precession angle. This corresponds to a 9° uncertainty in Φ. The effect of this on the polarization is well within the statistical uncertainties.

VII. Phase Shift Analysis

The analysis of our angular distribution into phase shift solutions incorporating the polarization data was performed by a computer program called KAPANAL, written by Dr. J. H. Foote and thoroughly described in his thesis.[16]

This program was a least squares grid search system to find a set of phase shifts that will give a minimum value of χ^2 for the experimental data, starting from a set of random numbers. One can start the minimization procedure over and over again with new sets of random numbers, thus eventually covering most of the χ^2 surface. The program has been adapted by Dr. Victor Cook, as is described in his thesis[4], and in the work of Cook et al.[5]

In the input data, other than the random numbers that form the starting point of the calculation, the following must be included: the ten differential cross section points from the angular distribution (Fig. 3), the four measured values of the differential polarization, $\overline{P_o}(\theta)_k^{cm}$, a total cross section estimate, and a total elastic cross section normalization estimate.

The last two items were obtained from other experiments in neighboring energy regions[3,4] by interpolation. No exhaustive attempt was made to measure cross sections, though two means were adopted to see that our data corroborated the conclusions of the other experiments. The first involved a tau decay scan[12] which gave the K^+ beam flux and showed that our total elastic cross section was within one standard deviation of the extrapolated value used in the program. The second method used a beam track study in sample film rolls to give a result about one and a half standard deviations away from the extrapolated value.

The cross sections used were:

$$\sigma_{(\text{total})} = 14.7 \pm 1.3 \text{ mb.}; \quad \sigma_{(\text{total elastic})} = 11.8 \pm 1.9 \text{ mb.}$$

From the cosine series fit to the angular distribution (Figs. 3 and 14) we see that the term of highest degree is $\cos \theta_k^{cm}$ or, possibly, $\cos^2 \theta_k^{cm}$. Thus, one would expect P-wave to be the highest angular momentum state needed to describe the interaction.

Yet, following the reasoning of Cook et al.[10], we allowed for a $D_{3/2}$ interaction since this corresponds to a possible N^* formation channel:

$$K^+ + P \rightarrow K + N^* \rightarrow K + N + \pi$$

(Threshold momentum: 880 MeV/c.) If one assumes the N^* production to take place in an orbital (K^+, N^*) S state, the $\frac{3}{2}+$ spin-parity assignment of the N^* requires the (K^+, P) system to have been in a $D_{3/2}$ state.

There is evidence from the work of Stubbs et al.[3] that some 60% of the inelastic interactions at a lower momentum (810 MeV/c) do take place through the reaction

$$K^+ + p \rightarrow K^o + \pi^+ + p.$$

Whether the (π^+, p) system can be described as the decay of an N^* is not clear. Although an attempt to ascertain this at our energy has been carried out[12], no conclusions are available at this time.

We made several attempts to include the absorption in all momentum channels and found in each case, however, that the clustering of solutions (on which we depend to discern the shape of the χ^2 surface) is smeared into a broad, general background. The same phenomenon, though less severe, occurred upon inclusion of the absorption in only two channels. Therefore, we decided that the problem was over

determined in the following sense. Each angular momentum channel tends to have definite solution clusters if only the real part of a given phase shift is included. If one asks for a fit of both the real and imaginary parts, these clusters tend to smear out.

It was decided, therefore, to limit absorption to one channel, though giving each channel the same number of random trials. Stubbs, et al.[3] had made the same decision and had found the results insensitive as to which channel was chosen.

Four hundred sets of solutions were obtained. There were 300 trials in the "S and P" category (100 for each of the three ways of including the absorption) and 100 trials of the "S-P-$D_{3/2}$" category. The first 50 trials in each category gave us nearly all the solutions; the last 50 brought these out again plus only two new ones, which were the sign changed solutions of some that had appeared previously. We concluded, therefore, that nearly all solutions had been found.

We obtained a chi-squared distribution whose shape fitted a theoretical curve very well, except that there seemed to be a lack of the very low chi-squared values $\left[P\ (\chi^2) > 0.75 \right]$. We chose a cut off at $P\ (\chi^2) = 0.01$.

To test the validity of this cut off we went back to the likelihood function given in section V, as modified in Appendix D:

$$\mathcal{L}(P_o) \propto \prod_i^k \left[(1 + P_o P_{l_i} \cos \Phi_i) \Big/ \int_{\Phi_{1_i}}^{\Phi_{2_i}} (1 + P_o P_{l_i} \cos \Phi)\, d\Phi \right].$$

In determining the polarization we maximized $\mathcal{L}(P_o)$ by inserting a range of values for P_o in this equation. We now changed this procedure in the following way. We first identified all the clusters of similar solutions from the phase shift fitting program, regardless of their χ^2 probability. Every solution predicts a polarization

function $P_o(\theta_k^{cm})$. We then inserted for each of the 94 events ($i = 1,2, \ldots 94$) its value of $\left[P_{o_j}(\theta_{k_i}^{cm})\right]$, as predicted by the j^{th} solution ($j = 1,2, \ldots 52$). Then $\mathcal{L}$ became the relative probability for the j^{th} solution:

$$\mathcal{L}(\delta_{s_j}, \delta_{p_{1/2_j}}, \ldots) \propto \prod_i^k \left[\frac{(1 + P_{o_j}\left[\theta_k^{cm}\right] P_{l_i} \cos \Phi_i)}{\int_{\Phi_{l_i}}^{\Phi_{2_i}} (1 + P_{o_j}\left[\theta_k^{cm}\right] P_{l_i} \cos \Phi)\, d\Phi} \right].$$

Likelihood rejection ratios can be set up. We considered that a ratio of 250:1 was sufficient to dismiss a particular solution.

This procedure is not independent of the KAPANAL program since the same polarization information is used in both; yet, there is a difference. KAPANAL uses a "lumped" polarization $\overline{P}_o$ over an angular region. The likelihood method, on the other hand, uses each event individually. The sensitivity of these methods is different. We therefore used the one as a check on the other.

All of the solutions rejected by χ^2 considerations were also rejected under our 250:1 likelihood rejection ratio. This is an indication that our χ^2 cut-off did not allow spurious solutions to enter. On the other hand, two or three solutions well within our likelihood tolerance were rejected by χ^2. In such cases we let χ^2 decisions prevail.

There were 37 solutions left after the χ^2 test. Next, error estimates were sought to detect overlap of solutions.

As explained in Foote's thesis[16], an error matrix involving the real parts of the phase shifts can be calculated by the KAPANAL program. This is based on an expansion of the χ^2 equation in a Taylor series at a minimum point where the first derivatives with respect to the parameters are zero. The inverse, G^{-1}, of the

matrix formed of second derivatives ($G_{ij} = (1/2)\frac{d^2[\chi^2]}{d\delta_i d\delta_j}$) is then shown to be the variance-covariance matrix. This assumes that higher terms of the Taylor series can be neglected, thus making χ^2 a quadratic function of the phase shifts near the minimum. Then

$$\Delta\chi^2 (\delta_1 \cdots \delta_n) = \sum_{i,j} G_{ij} \Delta\delta_i \Delta\delta_j$$

A set of small variations in the phase shifts then gives G_{ij} from the changes in χ^2. These variations, whose size can be set to any value, are made both in positive and negative directions ($\delta_i \pm \Delta\delta_i$). The value of G_{ij} is the average over the changes made. This renders G_{ij} less sensitive to the quadratic behavior assumption.

Another procedure used in KAPANAL is denoted as AUX by Foote. It is an auxilliary method of determining the variances and serves as a check on the error matrix calculation. Only one phase shift is varied at a time. The other phase shifts then adjust to obtain a new minimum of χ^2. From one such variation in δ_i one can determine the value of δ_i for which χ^2 will have changed by one unit. This distance $\left[\delta_i^{min} - \delta_i^{\chi^2 = 1}\right]$ is shown to correspond to the δ_i variance calculated from the error matrix. The value of this method is that it gives a geometrical interpretation to the χ^2 minimization process as motion inside a quadratic well[16]. This also, however, makes the method much more sensitive to the quadratic hypothesis.

In addition to these two methods, we employed a third as a check since both of these depended on quadratic behavior. We sought the clusters of solutions we had found previously and determined the variation among the same phase shifts in a given cluster. This relies on the real meaning of deviation as linked to the repetition

of the same experiment a large number of times.

All three methods corroborated each other's results. We adopted the values of deviations given by the error matrix because we found these to be insensitive to the exact size of the $(\Delta^2)_i$ steps taken.

Having found the r.m.s. errors in the phase shifts, we then eliminated the large amount of overlap in our 37 solutions. Two solutions were considered to be overlapping if they fell within two standard deviations of each other.

Another phenomenon had to be eliminated. Several strings of linked solutions, each about one standard deviation away from its neighbors, were found. They generally tended to some "best" solution at a low value of χ^2. In such cases, only the "best" solution, toward which all the others tended, was chosen. The linked chain was taken to describe a deep, but rough well, on the walls of which many spurious relative minima might appear.

Our final results consist of ten S and P wave solutions and six (S, P, $D_{3/2}$) wave solutions. These are presented in Table I.

The curve of predicted polarization $P(\theta_k^{cm})$ versus θ_k^{cm} for each of these solutions, along with the location of the four $\overline{P}_o$ measurements, is shown in Fig. 5.

VIII. Discussion

Three things have been accomplished here.

1. The angular distribution of K^+ - P scattering has been measured for 910 MeV/c and is presented in Fig. 3 with the best cosine series fits.

2. The polarization of the recoil proton has been measured from P-hydrogen and P-carbon scatters in the liquid of the chamber, and is presented in Figs. 5 and 18.

3. A phase shift analysis incorporating the polarization and angular distribution data has been undertaken, and the resulting solutions are shown in Table I.

As regards the angular distribution, it seems to show, as might be expected, a behavior mid-way between the near-isotropy of Stubbs et al.[3] at 810 MeV/c and the more pronounced forward peaking of Cook et al.[4,5] at 970 MeV/c. In this sense the three experiments, combined with the work of Cook et al.[4,5] at 1170 and 1970 MeV/c form a continuous series of transitions with increasing momentum.

As far as the polarization measurements are concerned they are mainly hampered by a lack of events. That propane is a good analyzing medium was shown by Fowler and Birge[8] and by Whatley[13], yet the present experiment has attempted to present in some detail all the relevant steps, including corrections and approximations, that are to be considered when polarization measurements are undertaken in a bubble chamber.

Turning now to the phase shift sets of Table I, we consider first the S-P solutions. Set (A^+, A^-), a ($P_{1/2}$ - $P_{3/2}$) mixture, was also found by Stubbs et al.[3] and by Cook et al.[4,5]. Set (B^+, B^-, B') represented our dominant S-wave solutions. S. Goldhaber et al.[1] found that negative S-wave phase shifts described their data, from 140 MeV/c at least as far as the 640 MeV/c region. δ_s decreased from - 10° at

140 MeV/c linearly with momentum to - 36° at 642 MeV/c. A δ_s of - 47° was also one of the results of Stubbs et al.[3]

We found the following situation with respect to solutions with large negative δ_s. There were numerous solutions of this type, but they all overlapped with a separation of one or, at most, two standard deviations. The solution labelled A^+, and included as a $(P_{1/2} - P_{3/2})$ mixture, was actually the solution of low χ^2 toward which all the linked solutions with negative δ_s tended. The opposite end of the chain is typified by solution B^- with its large errors. On the other hand, B' represents a solution that lies in the mid-point of the chain.

What this probably means is that the solutions with dominant $(-\delta_s)$ lie in a broad, deep, rough depression in the χ^2 surface with minimum at $\delta_s = 0$. The conclusion might be drawn from this that the K^+ - P interaction is no longer dominated by a repulsive S-wave phase shift, though we are prevented, probably by our large polarization errors, from seeing more positive indication of this.

Sets (C^+, C^-, C') and (D^+, D^-) are various dominant $\delta_{P_{1/2}}$ solutions. Some of these may be Minami ambiguities[17] of the B set, though ambiguities do not remain clearly identifiable in the presence of absorption. It is hard to link up these solutions with the low energy behavior, though similar sets were found by Stubbs et al.[3] and Cook et al.[4,5]

The D-wave solutions are presented in the second portion of Table I. No linking of chains of similar solutions was observed. The following were also found by Cook et al.[4,5]: E, F, H^+ and H^-.

In summary, then, the added polarization information raises a possibility that the dominant S-wave behavior of K^+ - P elastic scattering might have been superseded by a $(P_{1/2} - P_{3/2})$ mixture.

On the other hand a D-wave solution such as F offers a way of linking more easily to results at lower energy.

The disappearance of the dominant S-wave solution would be surprising but it appears as a very likely interpretation of this experiment.

Designation	δ_s	$\delta_{p_{1/2}}$	$\delta_{p_{3/2}}$	η	σ_{inel}	$P(\chi^2)$
A^+	0.6 ±2.0	-17.1 ±1.8	29.8 ±0.8	$\eta_s = 0.80$	1.8 mb	0.58
A^-	-5.5 ±1.5	20.3 ±2.2	-29.0 ±1.0	$\eta_{p_{3/2}} = 0.90$	1.9	0.01
B^+	44.6 ±3.8	-12.9 ±7.4	2.5 ±3.1	$\eta_{p_{3/2}} = 0.77$	4.1	0.22
B-	-41.2 ±24.5	-6.8 ±28.4	13.1 ±26.2	$\eta_{p_{3/2}} = 0.77$	4.1	0.22
B'	-27.0 ±13.3	-19.1 ±11.8	22.1 ±3.6	$\eta_{p_{3/2}} = 0.75$	4.4	0.25
C^+	-2.7 ±2.5	48.0 ±0.9	3.0 ±1.0	$\eta_s = 0.67$	2.8	0.07
C-	-5.4 ±1.8	-46.2 ±1.2	5.5 ±1.9	$\eta_{p_{3/2}} = 0.86$	2.6	0.14
C'	9.4 ±2.0	-57.9 ±7.0	15.2 ±3.2	$\eta_{p_{1/2}} = 0.50$	3.9	0.63
D^+	8.3 ±1.7	74.8 ±2.9	5.5 ±1.6	$\eta_{p_{1/2}} = 0.53$	3.8	0.45
D-	-5.6 ±1.9	-62.7 ±1.8	-1.1 ±1.8	$\eta_{p_{1/2}} = 0.65$	2.9	0.05

Solutions Involving S and P Waves

TABLE I

Designation	δ_s	$\delta_{p_{1/2}}$	$\delta_{p_{3/2}}$	$\delta_{D_{3/2}}$	$\eta_{D_{3/2}}$	$\sigma_{incl.}$	$P(\chi^2)$
E	23.7 ±7.7	22.4 ±7.5	1.2 ±0.9	-23.1 ±1.4	0.67	5.5 mb	0.29
F	-23.9 ±5.9	-24.0 ±2.4	18.9 ±2.8	-4.0 ±1.3	0.86	2.6	0.58
G^+	26.1 ±3.9	-5.1 ±3.1	2.2 ±1.3	-27.4 ±2.3	0.77	4.1	0.50
G^-	-18.3 ±2.2	4.6 ±2.1	0.5 ±1.2	29.3 ±0.9	0.99	0.2	0.01
H^+	2.6 ±2.9	-17.9 ±2.6	28.8 ±1.2	-3.6 ±1.4	0.84	3.0	0.29
H^-	5.0 ±3.5	19.5 ±2.2	-25.5 ±1.3	6.0 ±1.2	0.80	3.6	0.12

II. Solutions Involving S, P, and $D_{3/2}$ Waves

TABLE I

ACKNOWLEDGEMENTS

First thanks are due to Professor Wilson Powell for making the present experimental topic available to me, and for enabling me to use all the necessary personnel and facilities to accomplish the task.

Next, my special debt to Dr. George Gidal must be acknowledged. He was the immediately available guide and collaborator for most of this research.

Among the other physicists of the Powell-Birge Group, I mention Dr. Robert Birge, Dr. Anne Kernan, and Dr. Peter Newcomb for their help, especially on the subjects of polarization, statistics and general scattering theory, respectively.

For a good introduction to the KAPANAL program I am indebted to Dr. Victor Cook.

Mrs. Rho Gamow did nearly all of the original scanning and some of the editing of events and was an indispensable helper.

Many people were concerned in this experiment in the numerous phases of routine labor involved in sorting such a mass of data. Without their help the experiment would have been an enormous burden. I mention first the head of the data processing section for our group, Mr. Wes Weber, who was always extremely generous with his cooperation and help. The members of this section, whose work was of enormous aid to this experiment, are: Mrs. Marleigh Sheaff, Mr. David Hupp, and Mr. Anthony Thomas.

The Data Handling Group, headed by Mr. Howard White, handled the major computations. I wish to mention the cooperation of Mr. White and Mr. Dennis Hall, and -- for his patience, especially -- Mr. Loren Shalz.

I wish to thank Mrs. Toby Gidal for her generous assistance in FORTRAN programming.

For the labors of typing and for general helpfulness, my thanks go to Mrs. Nancy Wakeman.

Other people in our group also gave generous assistance in time of need. To all of these and to my fellow graduate students, I tender my appreciation and sincere thanks.

REFERENCES

1. S. Goldhaber, W. Chinowsky, G. Goldhaber, W. Lee, T. O'Halloran, T. F. Stubbs, G. M. Pjerrou, D. H. Stork, and H. K. Ticho, Phys. Rev. Letters 9, 135 (1962).

2. T. F. Kycia, L. T. Kerth, and R. G. Baender, Phys. Rev. 118, 553 (1960).

3. T. F. Stubbs, H. Bradner, W. Chinowsky, G. Goldhaber, S. Goldhaber W. Slater, D. M. Stork, and H. K. Ticho, Phys. Rev. Letters 7, 188 (1961).

4. V. Cook (Ph.D. thesis), K^+ - Nucleon Interactions in the Momentum Range of 800 to 2900 MeV/c, Lawrence Radiation Laboratory Report UCRL-10130, March 1962 (Unpublished).

5. V. Cook, D. Keefe, L. T. Kerth, P. G. Murphy, W. A. Wenzel and T. F. Zipf, Phys. Rev. 129, 2743 (1963).

6. G. Goldhaber, S. Goldhaber, J. Kadyk, T. F. Stubbs, D. Stork, and H. Ticho, Separated K^+ Beams, Lawrence Radiation Laboratory Report Bev-483, February 1960 (Unpublished).

7. W. M. Powell, W. B. Fowler, and L. O. Oswald, Rev. Sci. Instr. 29, 874 (1958).

8. R. W. Birge and W. B. Fowler, Phys. Rev. Letters 5, 254 (1960.

9. H. S. White, S. S. Buckman, D. E. Hall, E. Kurvitz, L. B. Meissner, J. C. Smith, and F. R. Stannard, The FOG, CLOUDY, and FAIR Programs for Bubble Chamber Data Reduction, Lawrence Radiation Laboratory Internal Report (Unpublished).

10. J. P. Berge, F. Solmitz, and H. D. Taft, Rev. of Sci. Instr. 32, 538 (1961).

11. T. G. Schumann, Lawrence Radiation Laboratory, Private Communication.

12. B. Kehoe, University of Maryland, Private Communication.

13. M. Whatley (Ph.D Thesis), Polarization in K^+ - P Elastic Scattering, University of Wisconsin 1962; also Bull. Am. Phys. Soc. Ser. II, 8 No. 1, 21 (1963).

14. A. E. Taylor, Reports on Progress in Physics XX (1957).

15. D. F. Nelson, A. A. Schupp, R. W. Pidd, and H. R. Crane, Phys. Rev. Letters 2, 492 (1959).

16. J. H. Foote (Ph.D. Thesis), Scattering of Positive Pions on Protons at 310 MeV; Recoil Nucleon Polarization and Phase Shift Analysis, Lawrence Radiation Laboratory Report UCRL 9191, Sept. 1960 (Unpublished).

17. J. Anderson and R. Golden, Ambiguities in Scattering Amplitudes, Lawrence Radiation Laboratory, Alvarez Memo 424, Oct. 1962 (Unpublished).

18. H. A. Bethe and P. Morrison, Elementary Nuclear Theory, 2nd ed. (John Wiley and Sons, New York, 1956).

19. J. Button, Use of the Density Matrix and Scattering Matrix in Calculating Intensities and Polarization in Some General Types of Interactions, Lawrence Radiation Laboratory, Alvarez Memo 337, Sept. 1961 (Unpublished).

20. L. Wolfenstein, Annual Reviews of Nuclear Science (1956).

21. J. Ashkin, Nuovo Cimento, Suppl. 2 to Vol XIV Ser. X (1959).

22. J. M. Blatt and V. F. Weisskopf, Theoretical Nuclear Physics (John Wiley and Sons, New York, 1952), Appendix.

23. L. I. Schiff, Quantum Mechanics, 2nd ed. (McGraw Hill, New York, 1955), Section 18.

24. J. A. Helland, T. J. Devlin, D. E. Hagge, M. J. Longo, B. J. Moyer, and C. D. Wood, Phys. Rev. Letters 10, 27 (1963).

APPENDICES

A. Angular Distribution and Polarization Formalism

A general presentation of spin 1/2 scattering formalism will be given in this section. The derivation follows closely that given in the book by Bethe and Morrison[18]. Reference is also made to the study of polarization in general interactions by J. Button[19] and to the article by Wolfenstein[19].

We can consider the K^+ - Proton interaction as an example of a wave with spin impinging on a spinless scattering center.

Such a wave can be denoted by the wave function

$$\psi_i = \begin{pmatrix} a_{1_i} \\ a_{2_i} \end{pmatrix} = a_{1_i}\,\varphi_1 + a_{2_i}\,\varphi_2, \tag{1}$$

where $\varphi_1 = \binom{1}{0}$ and $\varphi_2 = \binom{0}{1}$ are the two possible spin orientations along some arbitrary axis; and a_{1_i} and a_{2_i} are unspecified amplitude and phase factors.

The intensity of the wave is given by summing over the spin orientations

$$I = \sum_{i\,=\,1,2} \psi_i^{+}\,\psi_i = |a_1|^2 + |a_2|^2 \tag{2}$$

The degree of polarization along the axis of quantization is defined as the net fraction of spins that are aligned in this direction

$$P_z = \frac{N_{up} - N_{down}}{N_{up} + N_{down}} = \frac{|a_1|^2 - |a_2|^2}{|a_1|^2 + |a_2|^2} \tag{3}$$

We now introduce the density matrix defined as:

$$\rho_{ij} \equiv \psi_i \psi_j^{+} \quad ; \quad \rho = \begin{pmatrix} a_1 a_1^{*} & a_1 a_2^{*} \\ a_2 a_1^{*} & a_2 a_2^{*} \end{pmatrix} \tag{4}$$

Then we can write:

$$I = \text{trace } (\rho); \quad P_z = \frac{\text{trace } (\rho \sigma_z)}{\text{trace } (\rho)} \tag{5}$$

where we can also define P_x and P_y in a similar way.

A more general case is given by n incident waves where now ρ_{ij} is the average over the n density matrices each with its own weight. Any (2 x 2) matrix can be expanded as a linear combination of the unit matrix, $\vec{\vec{1}}$, and the three Pauli operators.

$$\vec{\vec{\rho}} = \frac{1}{2} I \left(\vec{\vec{1}} + \vec{P} \cdot \vec{\sigma}\right); \tag{6}$$

where

$$\vec{P} \cdot \vec{\sigma} = P_x \vec{\sigma}_x + P_y \vec{\sigma}_y + P_z \vec{\sigma}_z .$$

To verify that coefficients of the four matrices are indeed as given in Eq. (6) carry out the operations of Eq. (5), remembering the properties of products of Pauli matrices: (with cyclical rotation of subscripts)

$$\vec{\sigma}_x \vec{\sigma}_y = - \vec{\sigma}_y \vec{\sigma}_x = i\vec{\sigma}_z ;$$

$$\sigma_x \sigma_x = \vec{\vec{1}}$$

A general spin 1/2 wave, represented as a two element column vector, can be operated on by 2 x 2 matrices. In particular we may represent the scattering of such a wave as

$$\vec{\psi}_s = \vec{\vec{S}}\vec{\psi}_i \tag{7}$$

where $\vec{\psi}_i$ and $\vec{\psi}_s$ are incident and scattered waves, and S is the scattering matrix. (Then, omitting the vector and matrix designations)

$$\begin{aligned} \rho_i &= \psi_i \psi_i^+ ; \\ \rho_f &= \psi_s \psi_s^+ = S\psi_i \psi_i^+ S^+ = S\rho_i S^+ \end{aligned} \tag{8}$$

therefore we can write

$$I_i = \mathrm{tr}(\rho i); \; I_f = \mathrm{tr}\,(S\rho_i S^+) \tag{9}$$

The scattering matrix is an operator acting on an incident plane wave to produce an outgoing wave whose intensity is a measurable function of some chosen angles. Therefore, the scattering matrix

itself must contain the angular dependence since the incident plane wave does not. Thus I_f has an implicit angular dependence. The ratio of outgoing flux per solid angle to unit incoming flux is the differential cross section. This can be expressed by the fraction $\frac{I_f}{I_i}$. Therefore,

$$\frac{d\sigma}{d\Omega} = \frac{tr\ (S\rho_i S^+)}{tr(\rho_i)} \tag{10}$$

The scattering matrix, S, is (2 x 2) and can be expanded

$$\overrightarrow{\overrightarrow{S}} = (g)\ \overrightarrow{\overrightarrow{1}} + (h) \cdot \overrightarrow{\overrightarrow{\sigma}} \tag{11}$$

g must be a scalar or pseudo-scalar to preserve the (2 x 2) matrix form of $\overrightarrow{\overrightarrow{S}}$. h must be a vector or axial-vector because of the form of the $(h) \cdot \overrightarrow{\overrightarrow{\sigma}}$ term.

The present experiment deals with strong interactions in which parity is conserved, therefore we demand that

$$P\left[S(x,y,z)\right] = S(-x,-y,-z) = S(x,y,z)$$

Scalars and axial-vectors are even, while pseudo-scalars and vectors are odd, under the parity operation.

Consider now Eq. (11). $\overrightarrow{\overrightarrow{1}}$, the unit matrix, is unaffected by a parity operation. $\overrightarrow{\overrightarrow{\sigma}}$, the spin matrix, on the other hand, has the nature of angular momentum and is an axial vector. Both g and h then must be even under parity operations. Therefore h must be an axial vector and g must be a scalar.

The scattering is completely defined if we give the incident and outgoing momentum vectors in the system in which the target is at rest. Therefore, in general, both terms in $\overrightarrow{\overrightarrow{S}}$ will depend on these two pieces of information. We now form a scalar and an axial vector from $\vec{P}_{incident}$ and $\vec{P}_{outgoing}$:

$$g \propto \vec{P}_{in} \cdot \vec{P}_{out}; \quad \vec{h} \propto \vec{P}_{in} \times \vec{P}_{out}$$

Thus g and $|\vec{h}|$ are both functions of the magnitude of the two momenta and the scattering angle.

$$\vec{S} = g(P_{in}, P_{out}, \theta)\, \vec{1} + h(P_{in}, P_{out}, \theta)\, \hat{n} \cdot \vec{\sigma} \qquad (12)$$

where $\hat{n} = \dfrac{\vec{P}_{in} \times \vec{P}_{out}}{|\vec{P}_{in} \times \vec{P}_{out}|}$, the normal to the scattering plane defined by the momentum vectors.

We now have all the equations needed to formulate the problem.

Consider an incident wave along the +Z axis. $(\vec{P}_{in} \times \vec{P}_{out})$ must therefore be a vector in the (x,y) plane, and we place it along the y axis for convenience. Thus $\hat{n} = \hat{j}$. Further assume that the incident spin 1/2 wave is unpolarized. The assumption of stationary target is made in the usual phase shift analyses. The scattering angle, θ, is the same as in the center of mass system provided that the scattering center remains stationary throughout the interaction like a static potential well.

The density matrix, ρ_i, of the incident wave is then from Eq. (6) (omitting vector and tensor signs):

$$\rho_i = \frac{1}{2} I\, 1$$

The scattered matrix, ρ_f, is, from Eq. (8) and (12)

$$\rho_f = S\rho_i S^+ = \frac{1}{2} I(g\, 1 + h\hat{n} \cdot \sigma)\, (\widetilde{g\, 1 + h\hat{n} \cdot \sigma})^*$$

From Eq. (10):

$$\frac{d\sigma}{d\Omega} = \frac{\mathrm{tr}(S\rho_i S^+)}{\mathrm{tr}(\rho_i)} = |g|^2 + |h|^2 \qquad (13)$$

because $|h|^2 (n\cdot\sigma)\, (\widetilde{n\cdot\sigma})^* = |h|^2 |n_j|^2 \sigma_y \sigma_y^* = h^2$,

and because the trace of any of the Pauli matrices is zero.

From Eq. (5):

$$P = P_y = \frac{\mathrm{tr}\,(\rho_f \sigma_y)}{\mathrm{tr}(\rho_f)} = \frac{2\,\mathrm{Re}\, gh^*}{|g|^2 + |h|^2} \qquad (14)$$

$$P_x = P_z = 0$$

as can be seen by direct substitution in the relevant equations.

Thus we conclude that if polarization is induced in the first scatter, it must be in a direction normal to the scattering plane. We now find the expected angular distribution after second scattering,

$$\frac{d\sigma'}{d\Omega} = \frac{tr(\rho_f')}{tr(\rho_i')}$$

where

$$\rho_i' = \rho_f$$
$$S' = g'1 + h'n' \cdot \sigma$$
$$\rho_f' = S' \rho_i' S'^{+}$$

Here we have put n' as the normal to the second scattering plane. The angular distribution at the second scatter is

$$\frac{d\sigma'}{d\Omega} = \left[|g'|^2 + |h'|^2 \right] \left[1 + \frac{2 \, \mathrm{Re} \, g' h'^*}{|g'|^2 + |h'|^2} \, n' \cdot P \right] \tag{15}$$

The first bracket gives the angular distribution at the second scatter for an unpolarized incident beam. The second bracket is readily identified as $(1 + P' \cdot P)$ where $P' \cdot P$ is the dot product of the polarization vectors at the two scatters. P and P' are directed along n and n', respectively, the normals to the first and second scattering planes. Eq. (15) is usually written as

$$\frac{d\sigma'}{d\Omega} = I_{unpol} \, (1 + P_o P_1 \cos \Phi) \tag{16}$$

where P_o is the polarization induced at the first scatter; P_1 is the analyzing power of the second scatter; and cos Φ is the angle between the normals to the two planes of scattering. Eq. (13), (14), and (16) form the basis for the analysis of the present experiment.

B. Phase Shift Relations

We will now interpret the amplitudes g and h of equations (13) and (14) of Appendix A in terms of phase shifts. A good treatment of this subject will be found in Ashkin.[21]

Again we assume an incident plane wave carrying a spin of $\frac{1}{2}$ and moving along the +Z axis, the axis of quantization. We also assume a static spin zero potential well (a particle of spin zero moving along the negative Z axis gives the same results in terms of the scattering angles θ and φ).

This motion is described by the wave function

$$\psi_{inc} = e^{ikz} \begin{pmatrix} 1 \\ 0 \end{pmatrix} \qquad (1)$$

where we have assumed a $(+\frac{1}{2})$ spin projection. The scattering conserves the total angular momentum, J, in magnitude, $|\vec{J}|$, and direction, m_J. Parity is also conserved, which here implies the conservation of orbital angular momentum, $\vec{L}$. The total spin, $\vec{S}$, is conserved because only the proton carries spin.

The scattered wave, as $r \to \infty$ (which is the experimental limit), is assumed to be sinusoidal. In order to have the property that the number of scattered particles per unit area decrease as r^{-2} the wave must have an r^{-1} dependence. The assumption is made that as $r \to \infty$ the only observable difference between scattered and unscattered waves is a shift in phase (provided the scattering is elastic off a static potential well, since the wave length, or energy, in such a case cannot change).

The incident wave moving along the axis of quantization must have m_L, the L projection, equal to zero. Since m_s, the spin projection, is taken as $+\frac{1}{2}$ in Eq. (1), m_J (which is conserved) must

also be $+\frac{1}{2}$. The scattered wave then must have

$$m_L = m_J - m_s = (\tfrac{1}{2}) - (\pm \tfrac{1}{2}) = 0, 1.$$

Since the orbital angular momentum L is conserved, we expand Eq. (1) in a complete set of partial waves each an eigenfunction of some L state. Then to each L state correspond the two total angular momentum states $J = L \pm \frac{1}{2}$, which are conserved separately.

This is done with the aid of Clebsch-Gordon coefficients[22].

$$\psi_{inc.} = e^{ikz}\begin{pmatrix}1\\0\end{pmatrix} = \sum_{L=0}^{\infty} A_L(r)\, Y_L^{m_L=0}(\theta, \varphi)\begin{pmatrix}1\\0\end{pmatrix} \ldots . \qquad (2)$$

where $A_L = \sqrt{4\pi(2L+1)}\, i^L j_L(kr)$; $j_L(kr)$, a Bessel function, becomes

$$\frac{\sin\left(kr - \frac{L\pi}{2}\right)}{kr}$$

as $r \longrightarrow \infty$.

$$Y_L^{m_L=0} = \frac{1}{\sqrt{2L+1}}\left[\sqrt{L+1}\; y_{J=L+\frac{1}{2}} + L\; y_{J=L-\frac{1}{2}}\right]$$

Thus

$$\psi_{inc} = \sum_{L=0}^{\infty} A_L(r)\left[\frac{1}{\sqrt{2L+1}}\left(\sqrt{L+1}\; y_{J=L+\frac{1}{2}} + \sqrt{L}\; y_{J=L-\frac{1}{2}}\right)\right]\begin{pmatrix}1\\0\end{pmatrix} \qquad (3)$$

Each J state of the incident wave can be formed in only one way because m_L and m_s have been uniquely chosen. For the scattered wave, however, $m_L = 0$ or 1, and $m_s = \pm \frac{1}{2}$. Thus, for $m_J = +\frac{1}{2}$, each J state can be combined from two separate states: $(m_L = 0,\ m_s = +\frac{1}{2})$, and $(m_L = 1,\ m_s = -\frac{1}{2})$. Again we use Clebsch-Gordon coefficients:

$$y_{J=L+\frac{1}{2}} = \frac{1}{\sqrt{2L+1}}\left[\sqrt{L+1}\; Y_L^{m_L=0}\begin{pmatrix}1\\0\end{pmatrix} + \sqrt{L}\; Y_L^{m_L=1}\begin{pmatrix}0\\1\end{pmatrix}\right] \qquad (4)$$

$$y_{J=L-\frac{1}{2}} = \frac{1}{\sqrt{2L+1}}\left[\sqrt{L}\; Y_L^{m_L=0}\begin{pmatrix}1\\0\end{pmatrix} - \sqrt{L+1}\; Y_L^{m_L=1}\begin{pmatrix}0\\1\end{pmatrix}\right]$$

The scattered wave function beyond the potential well is given by the difference between the total wave function and the undeflected part.

The undeflected part is given by Eq. (3)*. The total wave function is required to differ from Eq. (3) only in phase, therefore, we multiply all the terms in the summation by

$$\left[e^{2i\delta_{L,J}}\right]$$

We set

$$\left[e^{2i\delta_{L,J-1}}\right] = A_{L,J}.$$

$$\psi_{scatt.} = \sum_{L=0}^{\infty} A_L(r) \left[\frac{1}{\sqrt{2L+1}} \left(\sqrt{L+1}\, A_{L,J=L+\frac{1}{2}}{}^{y}{}_{J=L+\frac{1}{2}} + \sqrt{L}\, A_{L,\,J=L-\frac{1}{2}}{}^{y}{}_{J=L-\frac{1}{2}}\right)\right] \quad (5)$$

where

$$A_L(r) = \left[\frac{e^{ikr}}{r}\right] \frac{\sqrt{4\pi\,(2L+1)}}{2\,ik}$$

as $r \to \infty$.

We can substitute Eq. (4), which applies to the scattered wave, into Eq. (5). Then we separate $f(\theta, \varphi)$, that portion of $\psi_{scatt.}$ that does not depend on r, because we want

$$\frac{d\sigma}{d\Omega} = |f(\theta,\varphi)|^2$$

the angular distribution of scattered particles[23].

---

* $A_L(r)$ in Eq. (3) as $r \to \infty$ becomes $\sqrt{\frac{4\pi(2L+1)}{2ikr}} \left(e^{i\,kr} - (-1)^L e^{-\,ikr}\right)$

The second term in the parenthesis, representing an incoming wave at infinity is not physically meaningful, and is omitted. $A_L(r)$ then has the required form.

Then, on arranging these terms we get

$$\frac{d\sigma}{d\Omega} = |g(\theta,\varphi)|^2 + |h(\theta,\varphi)|^2 \tag{6}$$

where

$$g(\theta,\varphi) = \frac{\sqrt{4\pi}}{2ik} \sum_{L=0}^{\infty} \frac{1}{\sqrt{2L+1}} \left[(L+1) A_{L,\, L+\frac{1}{2}} + L A_{L,\, L-\frac{1}{2}} \right] Y_L^0(\theta,\varphi) \begin{pmatrix} 1 \\ 0 \end{pmatrix}$$

$$h(\theta,\varphi) = \frac{\sqrt{4\pi}}{2ik} \sum_{L=0}^{\infty} \sqrt{\frac{L(L+1)}{2L+1}} \left[A_{L,\, L+\frac{1}{2}} - A_{L,\, L-\frac{1}{2}} \right] Y_L^1(\theta,\varphi) \begin{pmatrix} 0 \\ 1 \end{pmatrix} \tag{7}$$

That this procedure is valid for relativistic particles obeying the Dirac equation has been shown by Ashkin[21].

Coulomb scattering has not been included here. It has been treated in detail by Dr. J. H. Foote[16].

That $g(\theta,\varphi)$ and $h(\theta,\varphi)$ are indeed the g and h of Appendix A is shown as follows:

$$\overleftrightarrow{S}\begin{pmatrix} 1 \\ 0 \end{pmatrix} = (g \overleftrightarrow{1} + h \vec{n} \cdot \vec{\sigma}) \begin{pmatrix} 1 \\ 0 \end{pmatrix}$$

This was the form of the scattering matrix used, where n is a vector normal to the plane of scattering, and lies therefore in the (x,y) plane. We assumed, $\hat{n} = \hat{j}$, that $\hat{n}$ lay along the y-axis. Then $n \cdot \sigma = \sigma_y$.

$$S\begin{pmatrix} 1 \\ 0 \end{pmatrix} = \left[g \begin{pmatrix} 1 & 0 \\ 0 & 1 \end{pmatrix} + h \begin{pmatrix} 0 & -i \\ i & 0 \end{pmatrix} \right] \begin{pmatrix} 1 \\ 0 \end{pmatrix} = \begin{bmatrix} g & -ih \\ ih & g \end{bmatrix} \begin{pmatrix} 1 \\ 0 \end{pmatrix} = \begin{pmatrix} g \\ ih \end{pmatrix}$$

This can be written

$$S\begin{pmatrix} 1 \\ 0 \end{pmatrix} = g\begin{pmatrix} 1 \\ 0 \end{pmatrix} + ih\begin{pmatrix} 0 \\ 1 \end{pmatrix} \tag{8}$$

g is the non-spin-flip term, and h is the spin-flip term. Thus Eq. (6) has the same significance as Eg. (13) of Appendix A.

The spherical harmonics Y_L^m are expressible in sinusoidal functions. Thus Eq. (6) can be expanded in a cosine series: $A + B\cos\theta + C\cos^2\theta + \ldots$

The experimental procedure is to measure the angular distribution of scattered particles, then to fit the data with a cosine series. From

the degree of the terms one can roughly estimate to what order in L the series of Eq. (6) is to be carried.

Any dynamical theory of the K^+ - P interaction that arises must then be tested by being able to reproduce this set of phase shift.

C. Spin Precession

We wish to measure the spin polarization induced on the recoil proton at the first (K^+ - P) vertex, in a direction normal to the plane of scattering. The relativistic precession of this spin component, as the proton moves in the magnetic field of the bubble chamber to the second (analyzing) vertex, is composed to two parts. The spin precesses simultaneously about the direction of the magnetic field and about the direction of the velocity. Since the proton velocity vector, $\vec{v}$, itself curves in the field at the frequency $\left[\omega_c = \frac{eB}{\gamma mc}\right]$, this precession about the velocity is a continuously varying quantity. The precession about the magnetic field, $\vec{B}$, will also vary continuously if the magnitude and direction of $\vec{B}$ are not constant over the trajectory. In addition, both components are affected by a continuous decrease in the magnitude of the velocity, $|\vec{v}|$, as the proton moves in the propane. In general, then, the total angle of precession for a given trajectory must be denoted by an integral over all these quantities.

For the purposes of this experiment it is sufficient to use an approximate formula since we can neglect all effects that are small compared with the uncertainties due to our relatively low statistics.

We use the formula derived by G. W. Ford[15] and adapted by Fowler and Birge[8].

$$\vec{\omega}_o = \frac{e\vec{B}}{m\gamma c}\left[1 + \left(\frac{g}{2} - 1\right)\gamma\right] - \frac{\vec{v}}{|\vec{v}|}(\gamma - 1)\left(\frac{g}{2} - 1\right)\left(\left[\frac{e\vec{B}}{m\gamma c}\right]\cdot\left[\frac{\vec{v}}{v}\right]\right)$$

Where $\vec{\omega}_o$ is the vector sum of the precession about $\vec{B}$ and $\vec{v}$; $\frac{e}{m}$ is the charge to mass ratio for the proton; γ is the relativistic contraction factor $\left(1 - \frac{v^2}{c^2}\right)^{-\frac{1}{2}}$; $\frac{g}{2} = \mu = 2.79$ is the magnetic moment of the proton; and c is the speed of light.

First, we consider the size of the second term, the precession about the velocity, in relation to the first. We rewrite Eq. (1) in terms of the magnitudes of the vectors, calling the first term $\vec{\omega}_B$ and the second term $\vec{\omega}_v$.

$$|\vec{\omega}_o|^2 = |\vec{\omega}_B|^2 + |\vec{\omega}_v|^2 + 2|\vec{\omega}_B|\ |\vec{\omega}_v| \cos \sphericalangle (\vec{v}, \vec{B})$$

$$|\omega| = \frac{|\Delta\beta|}{|\Delta t|}$$

where β is the precession angle.

Setting the factor $(\vec{B} \cdot \frac{\vec{v}}{|\vec{v}|})$ in Eq. (1) to its maximum value,

$$R = \frac{|\Delta\beta_v|}{|\Delta\beta_B|} = -\left[\frac{\gamma - 1.000}{\gamma + 0.559}\right] \quad ; \qquad \text{and} \qquad (4)$$

$$|\Delta\beta_o| = \left[1 + R^2 + 2R \cos \sphericalangle (v, B)\right]^{\frac{1}{2}} |\Delta\beta_B| \qquad (5)$$

The maximum proton momentum at the first $(K^+ - P)$ elastic scatter puts an upper limit on R such that R^2 is always less than 0.077. The term $|2 R \cos \sphericalangle(\vec{v},\vec{B})|$ has a maximum value of 0.20 at a momentum of 900 MeV c and $|\sphericalangle(\vec{v}, \vec{B})|$ of 60°. Therefore

$$|\Delta\beta_o|_{max} = 1.13\ |\Delta\beta_B| \text{ for } \sphericalangle(v, B) = 120^\circ \qquad (6a)$$

$$|\Delta\beta_o|_{min} = 0.94\ |\Delta\beta_B| \text{ for } \sphericalangle(v, B) = 60^\circ \qquad (6b)$$

If the direction of $\vec{B}$ is vertical, Eq. (6a) and (6b) refer to particles scattered downward and upward by 30°, respectively, from the horizontal.

If now, we neglect the $|\Delta\beta_v|$ contribution to the precession, we set

$$|\Delta\beta_o| = \Delta\beta_B|$$

We then find that the percentage error is

$$\frac{\delta_1(|\Delta\beta_o|)}{|\Delta\beta_o|} = \begin{cases} + 11.5\% \\ - \ 6.4\% \end{cases} \qquad (7)$$

As our next step we consider the magnetic field uncertainty.

We find

$$\frac{\delta_2 (|\Delta\beta_o|)}{|\Delta\beta_o|} = \frac{\delta|\vec{B}|}{|\vec{B}|} = \pm 10\%$$

from the known characteristics of the bubble chamber magnet. The direction of $\vec{B}$ is found to be very nearly constant.

Finally, we consider the effect introduced by the proton's energy loss in propane between first and second scatters. Assuming the precession component about $\vec{v}$ to have been neglected, we have from Eq. (3)

$$|\Delta\beta_o| = \frac{eB}{m\gamma c} (1 + 1.79\gamma) (\Delta t)$$

This time, Δt, spent in moving between first and second scatters is

$$\Delta t = \frac{L}{v}$$

where L is the distance travelled.

Then $$|\Delta\beta_o| = \frac{eBL}{mc^2} \left(\frac{mc}{p} + \frac{1.79}{\beta_v} \right) ; \qquad (9)$$

where P is the momentum of the proton and $\beta_v = \frac{v}{c}$.

Using the equalities

$$P = \beta_v \gamma mc,$$

$$\beta_v^2 = \frac{1}{1 + \frac{m^2c^2}{p^2}}$$

$$\frac{\delta\beta_v}{\beta_v} = \left[\frac{1}{1 + \frac{p^2}{m^2c^2}} \right] \frac{\delta p}{p}$$

we find

$$\frac{\delta_3 (|\Delta\beta_o|)}{|\Delta\beta_o|} = - \left(\frac{1 + 1.79\gamma \left(\frac{1}{1 + \frac{p^2}{m^2c^2}} \right)}{1 + 1.79\gamma} \right) \frac{\delta p}{p} \qquad (10)$$

If instead of using the initial value of momentum, we had used the average value as a better approximation, at worst the change would have been 11.5%.

From Eq. (7), (8), and (10) we find that -- should δ_1, δ_2, and δ_3 operate in the same direction -- our maximum precession angle error would amount to about 33%. A corresponding error would be introduced in the value of cos Φ.

Let us estimate the maximum precession angle from Eq. (9)

$$|\Delta\beta_o|_{max} = \frac{eBL_{max}}{mc^2}\left(\frac{mc^2}{P_{min}c} + \frac{1.79}{\beta_{v_{min}}}\right)$$

The maximum values of the terms $\left[L_{max}\left(\frac{mc^2}{P_{min}c}\right)\right]$ and $\left[L_{max}\ \frac{1.79}{\beta_{v_{min}}}\right]$ occur for essentially the same values of the parameters, namely: L_{max} = 44 cm, P_{min} = 600 Mev. Then

$$|\Delta\beta_o|_{max} = 0.47_{radians} = 27^o$$

Thus, our maximum error, due to the omission of the corrections discussed earlier, will be less than 9^o. As defined in the text cos $\Phi = \hat{n}_1 \cdot \hat{n}_2$. $\hat{n}_1$ is the precessing vector. The error is $\Delta\beta_o$ will have maximum effect if the precession axis is normal to the $(\hat{n}_1, \hat{n}_2)$ plane. Then

$$\delta(\Delta\beta_o) = \delta\Phi$$

If $\Phi = 0$, the 9^o error will introduce a change of 0.012 in cos Φ. If $\Phi = 90^o$, the change in cos Φ is 0.156. This can give

$$\left(\frac{\delta P_o}{P_o}\right)_{max} \cong \pm\ 0.20$$

The smallest polarization error quoted in this experiment is ± 0.45. This justified omission of the corrections discussed in this appendix.

D. The Whatley Correction

The purpose of this correction has been explained in the text. The procedure will be discussed here.

The situation, briefly, is this. Assume a proton recoiled from the K^+ - P interaction moving toward one of the surfaces (top or bottom glass plates) of the bubble chamber. Shortly before it would have left the chamber, it interacts again and scatters off at angles α ,β. For polarization measurements the azimuthal angle β(measured about the direction of the incident proton at the second interaction determines the orientation of the second scattering plane relative to the first. It is an asymmetry in β that indicates that the proton was polarized. Therefore, all β orientations must be visible. Some β directions may be obscured in the sense that a proton scattering through an angle α near the top plate may be deflected downward back into the chamber (to leave a long, easily seen track), or upward out of the chamber (leaving an invisibly short track). Such invisible regions of scattering will give a false asymmetry. In the likelihood function described in the text, where $(1 + P_o P_1 \cos \Phi)$ is computed individually for each event, we must also individually correct each event for these invisible β regions. We now consider a geometrical way of doing this. In Fig. 19 where the following series of steps is illustrated.

On tracing paper make a scale drawing of a vertical section through the bubble chamber.

Plot on this the position of the second scattering vertex.

Place a Wolfe chart beneath the tracing paper, centered at the vertex point. A Wolfe chart is a two dimensional representation of

of a sphere with longitudes and latitudes marked off. The outline of one quadrant of such a chart is included in Fig. 19. The abscissa is marked off in longitude from 0° to 90° and from 270° to 360° denoting the back and the front of the sphere, respectively. The chart is so aligned that 90° dip and 0° or 360° azimuth point in a direction parallel to the top glass of the bubble chamber.

Plot the angular position of the vectors corresponding to the proton P_o and of the scattered proton P_{sc} on the Wolfe chart.

Find the space angle, $\sphericalangle(P_oP_{sc})$, between P_o and P_{sc} by rotating the Wolfe chart about its center so that these two points lie on the same great circle arc. This great circle arc may pass over the pole if P_o and P_{sc} lie on opposite sides of the sphere.

Find the locus of all points (leaving P_o stationary) that lie as far away in angle from P_o as P_{sc} does. This involves passing successive great circle arcs through P_o. The locus of these points form the crescent in Fig. 19.

The locus just drawn is the intersection of a cone of half angle $\sphericalangle(P_o, P_{sc})$ with the Wolfe chart sphere. It represents all possible azimuthal orientations of the scattered proton. We must now decide what projected length would be too short to be seen in the photographs. This varies with the region of the chamber, with azimuthal orientation, and with the angle of scattering. Since we find many P-C events with small scattering angles where P_{sc} must be rather long to be detected, we choose a cut off length of 9 mm.

We now draw a line through the vertex point (x,z) and through the point $(x' = x + 9 \text{ mm}; Z' = Z_{\text{top glass}})$.

If no part of the locus lies to the right of the line just drawn all orientations for this event will leave x projections greater than 9 mm.

Yet, even if the x projection is less than 9 mm., the (x, y) plane projection may be of acceptable length. To find the shortest (x, y) plane projection, find the point on the locus that corresponds to the most nearly vertical dip angle, θ^{min}. Then

$$L_{(x,y)_{min}} = (Z_{top\ glass} - Z_{vertex}) \tan \theta^{min}$$

If $L_{(x,y)_{min}} < 9$ mm, we must find the limits of the visible portion of the locus. We find the steepest dip angle θ_{dip} that still gives visible tracks:

$$\tan \theta_{dip} = \frac{0.9 \text{ cm}}{(Z_{top\ glass} - Z_{vertex})}$$

We then follow the parallel of latitude at the value of θ_{dip} until it intersects the locus. There are usually two such intersections, which are labelled X_1 and X_2 in Fig. 19. The portion of the locus lying between X_1 and X_2 and to the right of the line drawn from (x,z) to (x + 9 mm, $Z_{top\ glass}$) is the region of invisibly short projections.

We now consider the connection between the invisible region and the likelihood function. For this we must find the normal to the scattering plane at the first vertex.

Place the angular coordinates of the incoming K^+ labelled K_{in} in Fig. 19 on the Wolfe chart.* Find the normal to the first scattering plane $\hat{n}_1 \propto \left| \vec{K}_{in} \times \vec{P}_o \right|$.

A cross product vector can be found by placing the points K_{in} and P_o on the same great circle arc. This great circle is the intersection of the plane defined by $\vec{K}_{in}$ and $\vec{P}_o$ with the Wolfe chart sphere. $\hat{n}_1$ is then normal to this, at the vertex -- that is, $\hat{n}_1$ lies $\pm 90^o$ away

---

* It is assumed that the curving of P_o in the magnetic field and the spin precession have been compensated for by changing the K_{in} azimuthal position.

from the great circle, in azimuth, and at the position of the equator in dip, both being referred to that position of the Wolfe chart in which K_{in} and P_o lie on the same great circle arc. The (±) sign enables us to locate either $(\vec{K}_{in} \times \vec{P}_o)$ or $(\vec{P}_o \times \vec{K}_{in})$.

In the likelihood function, cos Φ is defined as the projection of $\hat{n}_1$ on the normal to the second scattering plane $\hat{n}_2$.

To find the invisible regions of cos Φ take the cross products $\hat{n}_2 \propto (\vec{P}_o \times \vec{X}_1)$ and $\hat{n}_3 \propto (\vec{P}_o \times \vec{X}_2)$ where $\vec{X}_1$ and $\vec{X}_2$ are the two intersections described above. Since $\hat{n}_1$, $\hat{n}_2$ and $\hat{n}_3$ are normal to $\vec{P}_o$, they will all lie in the same plane, and hence on the same cirle arc. Rotate the Wolfe chart until this is seen to occur. Then define Φ_1 as the $\sphericalangle(\hat{n}_1, \hat{n}_2)$ and Φ_2 as the $\sphericalangle(\hat{n}_1, \hat{n}_3)$. These two values of the angle Φ will delineate the limits of the visible region

It may happen occasionally that the actual point P_{sc} will fall in the so-called invisible region. This will indicate that the 9 mm cut-off, for instance, is too large. Yet, it is almost impossible, considering all possible positions and orientations of tracks, to find an absolute cut-off limit. All events that fall in the invisible region must be rejected.

About 4% of the events considered for the Whatley correction fell in this category.

We now discuss the correction of the likelihood function

Consider first the case of an event that does not need the correction. Since all azimuthal orientations of P_{sc} will be detected, this event has no bias. An event with an invisible Φ region, however, must be assigned <u>less</u> of a role in the polarization determination since a

scattering in another azimuthal direction would have been missed. The fact that P_{sc} was seen is useful knowledge, but less useful than had all orientations been visible.

On the other hand, since with an invisible region the probability of seeing P_{sc} at all is less than for normal events, the fact that we actually observed it must be given greater absolute weight.

Thus an event with some orientations obscured must be given greater absolute weight for having appeared at all, yet it must receive less of a role in the polarization determination.

These two things can be done simultaneously because of a property of the likelihood function already described in the text. We can multiply it by any constant probability factor we choose without affecting its behavior with respect to the polarization. Multiplying an event by some large factor does not preclude that this event will nevertheless have less of a role in the polarization determination.

The final form of the likelihood function is

$$\mathcal{L}(P_o) \propto \prod_i^k \left(\frac{1 + P_o P_{l_i} \cos \Phi_i}{\int_{\Phi_{l_i}}^{\Phi_{2_i}} (1 + P_o P_{l_i} \cos \Phi)\, d\Phi} \right) \tag{1}$$

where the integral ranges over the visible region.

This form has the two properties discussed above. In the limit of shrinking visible region,

$$(\Phi_{2_i} - \Phi_{l_i}) = \Delta\Phi_i \to 0^o,$$

the term for the i^{th} event becomes:

$$\mathcal{L}_i \sim \frac{(1 + P_o P_{l_i} \cos \Phi_i)}{(1 + P_o P_{l_i} \cos \Phi_i) \int_{\Phi_l}^{\Phi_2} d\Phi} = \frac{1}{\Delta\Phi_i} \to \infty \text{ as } \Delta\Phi_i \to 0.$$

It has been assumed here that the integrand is constant over the small interval $\Delta\Phi_i$. Thus the i^{th} event ($\mathcal{L}_i$) multiplies $\mathcal{L}$ by a nearly infinite scale factor, yet $\mathcal{L}_i$ is totally insensitive to the polarization and contributes nothing to its determination.

This states, also, the known fact that a scintillation counter experiment with only one detection position cannot measure a polarization. The scattered proton must have an alternative of scattering into more than a single azimuthal direction.

Eq. (1) is the corrected form of the likelihood function used in this experiment.

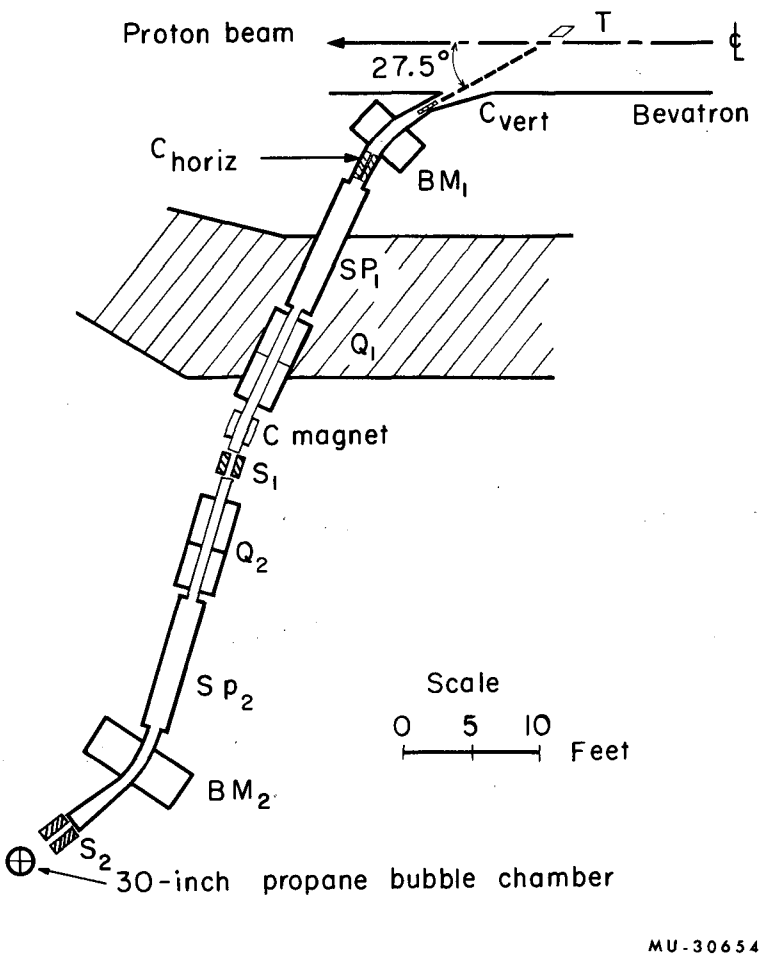

Fig. 1(a). Experimental beam arrangement.

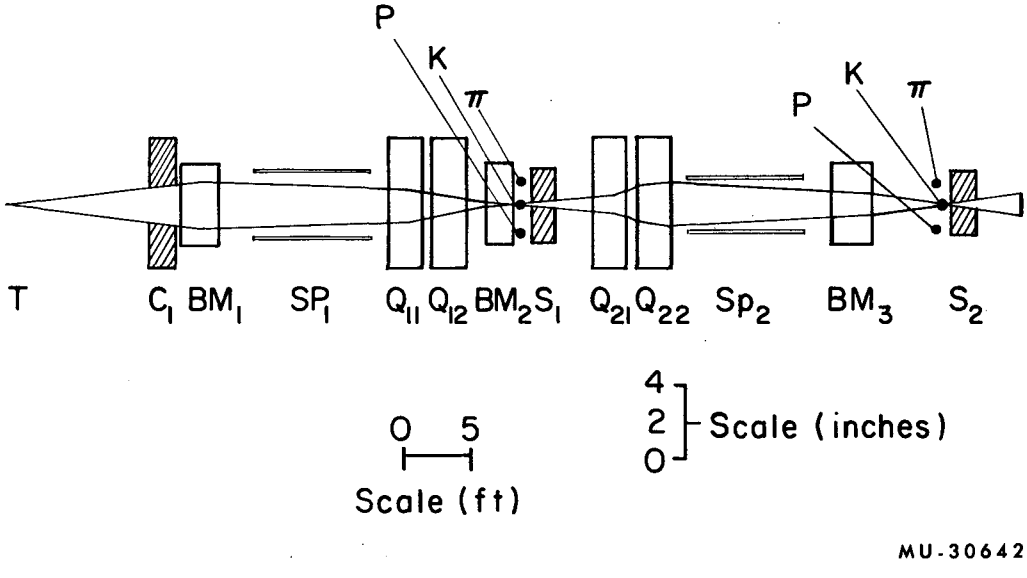

Fig. 1(b). Vertical lens and focussing diagram.

ZN-3822

Fig. 2. An example of K^+-proton elastic scattering.

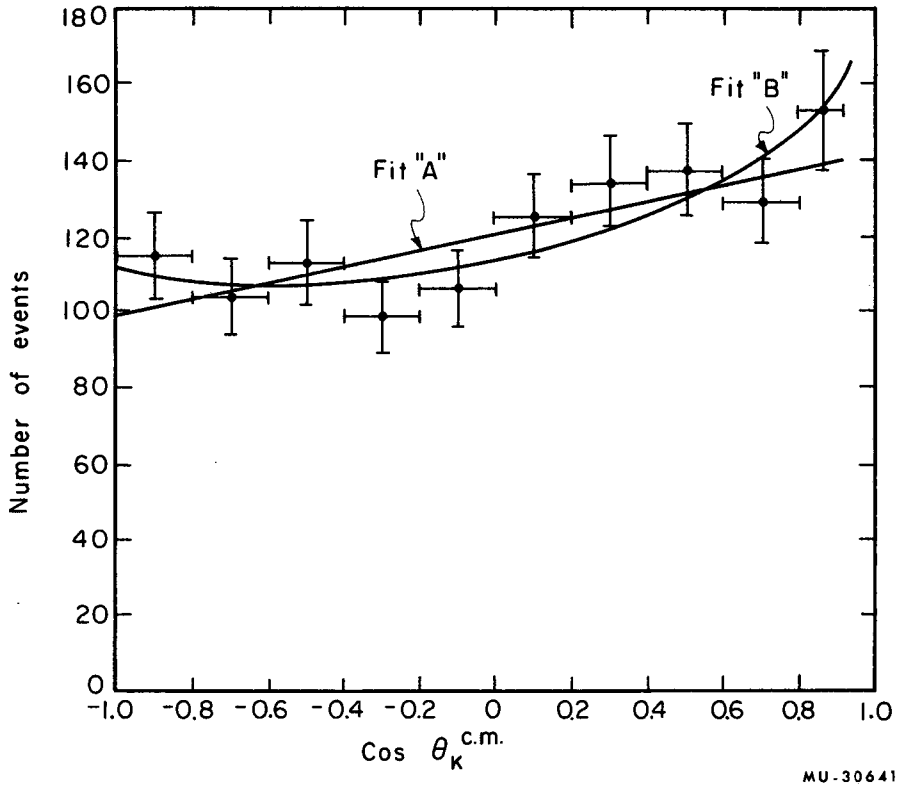

Fig. 3. Experimental angular distribution at 910 MeV/c based on 1154 events. Fit "A" is $(1 + a \cos \theta_K^{cm})$. Fit "B" is $(1 + b \cos \theta_K^{cm} + c \cos^2 \theta_K^{cm})$ where $a = 0.18 \pm 0.05$; $b = 0.20 \pm 0.06$; $c = 0.18 \pm 0.12$.

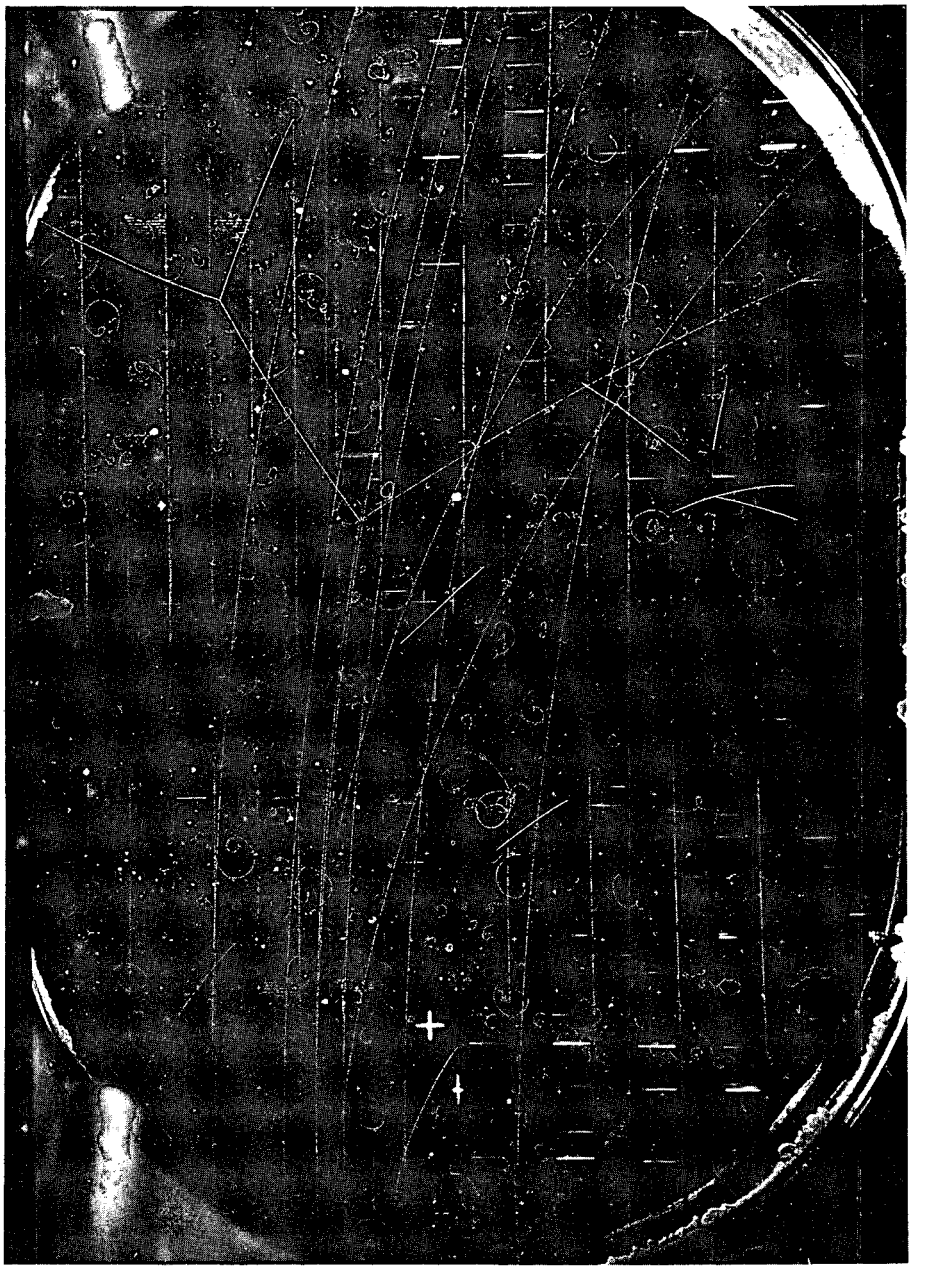

ZN-3821

Fig. 4(a). An example of K^+-P elastic scattering followed by a P-hydrogen elastic scatter.

ZN-3820

Fig. 4(b). An example of K^+-P elastic scattering followed by a P-carbon interaction.

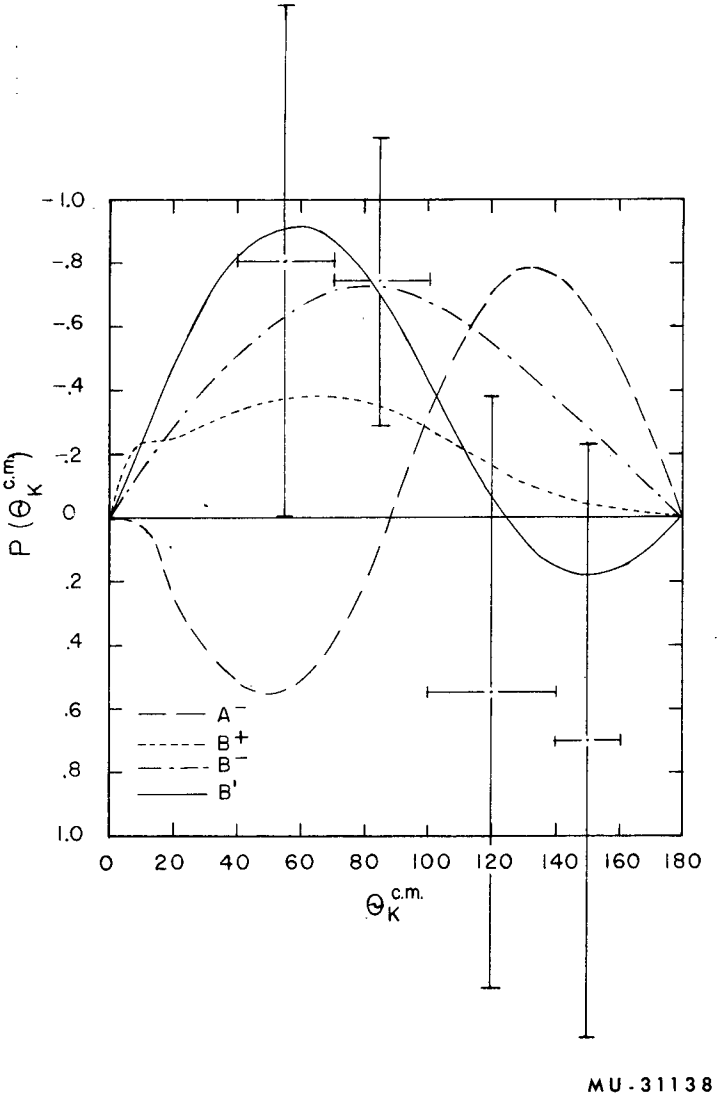

Fig. 5(a). Differential polarization curves for solutions in Table I with measured values of polarization superimposed. The $P(\chi^2)$ probabilities of Table I reflect goodness of fit both polarization and angular distribution data. The effect of the polarization data is shown in the low $P(\chi^2)$ values assigned, for instance, to solutions A^-, G^-, and H^-.

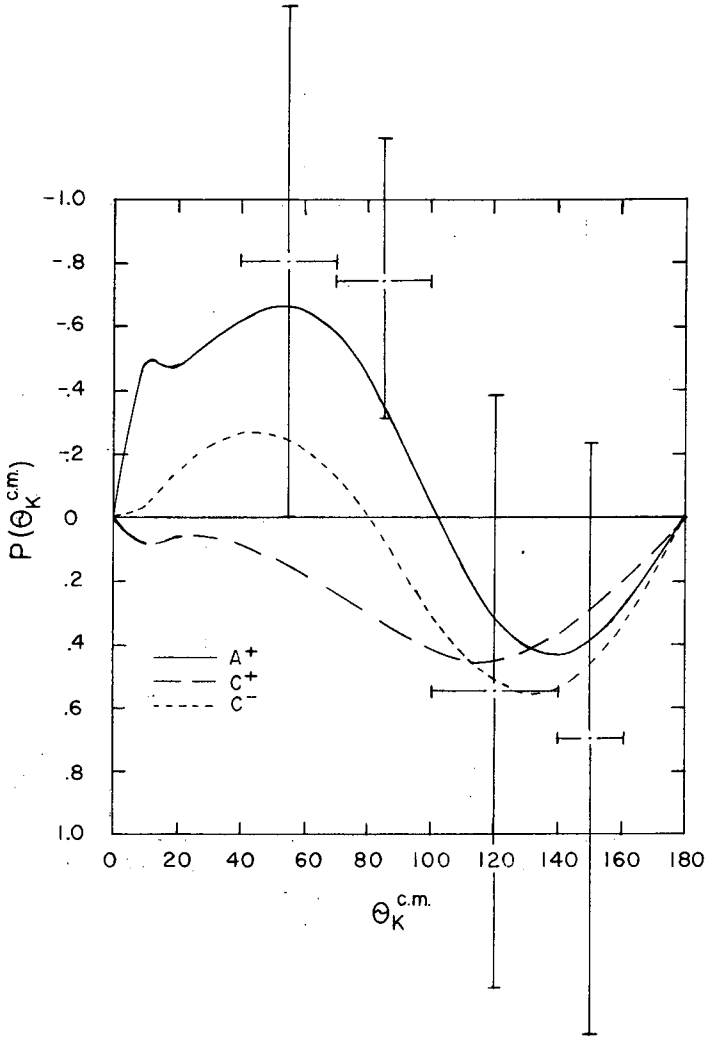

Fig. 5(b). Differential polarization curves [see caption of Fig. 5(a)].

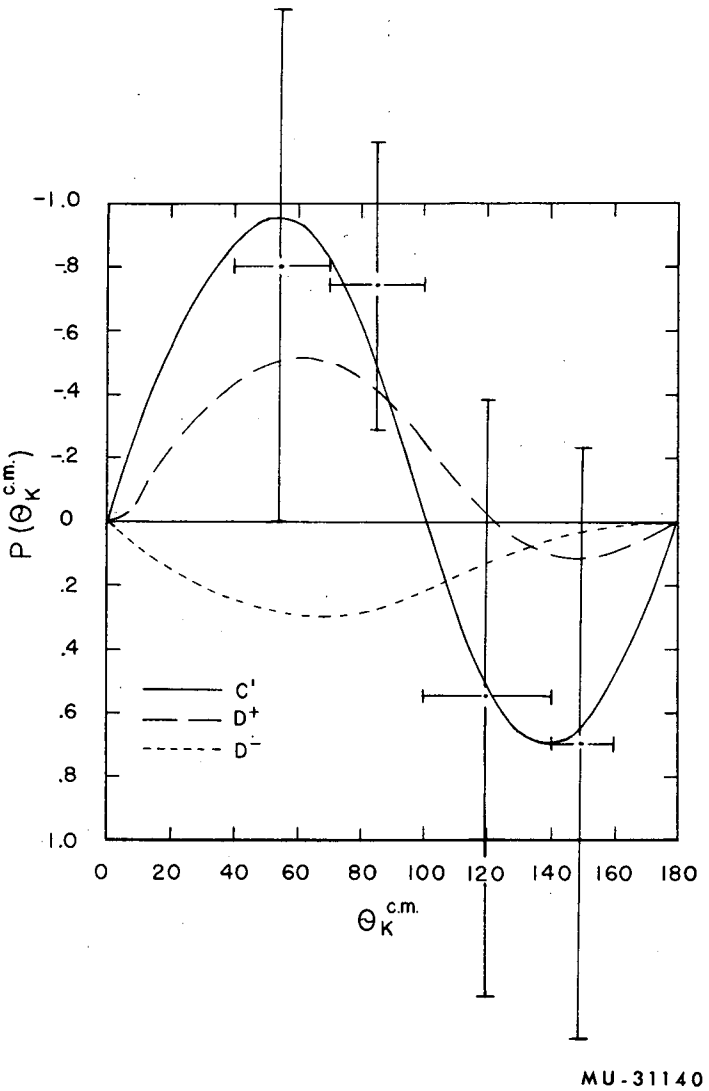

Fig. 5(c). Differential polarization curves [see caption of Fig. 5(a)].

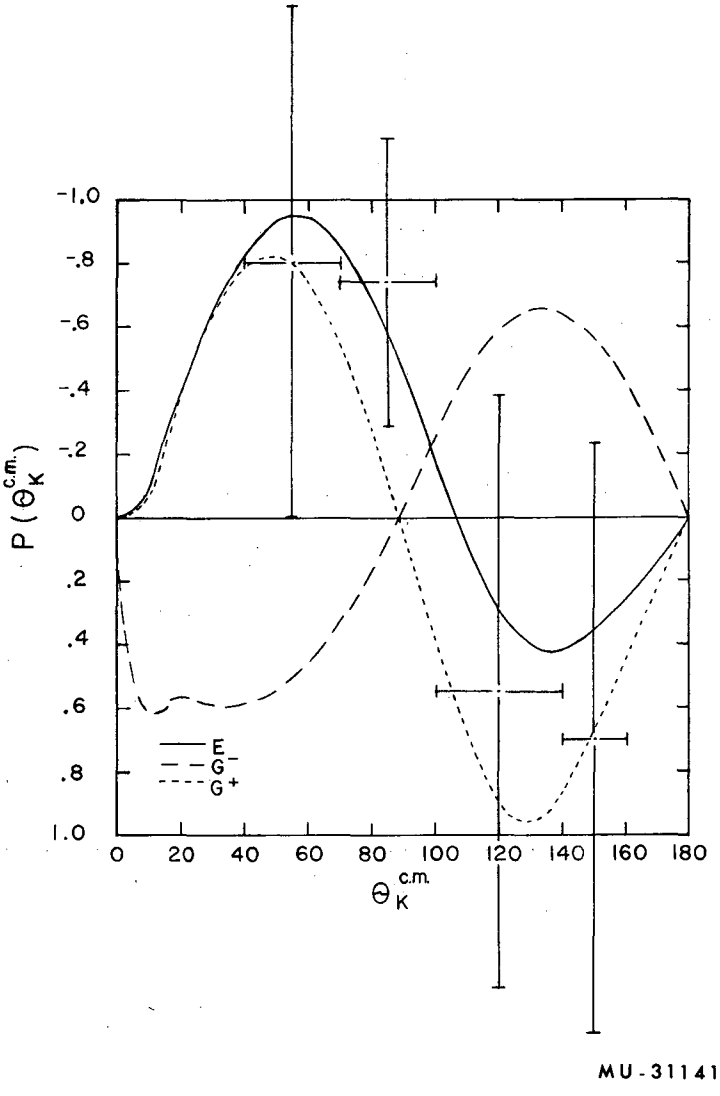

Fig. 5(d). Differential polarization curves [see caption of Fig. 5(a)].

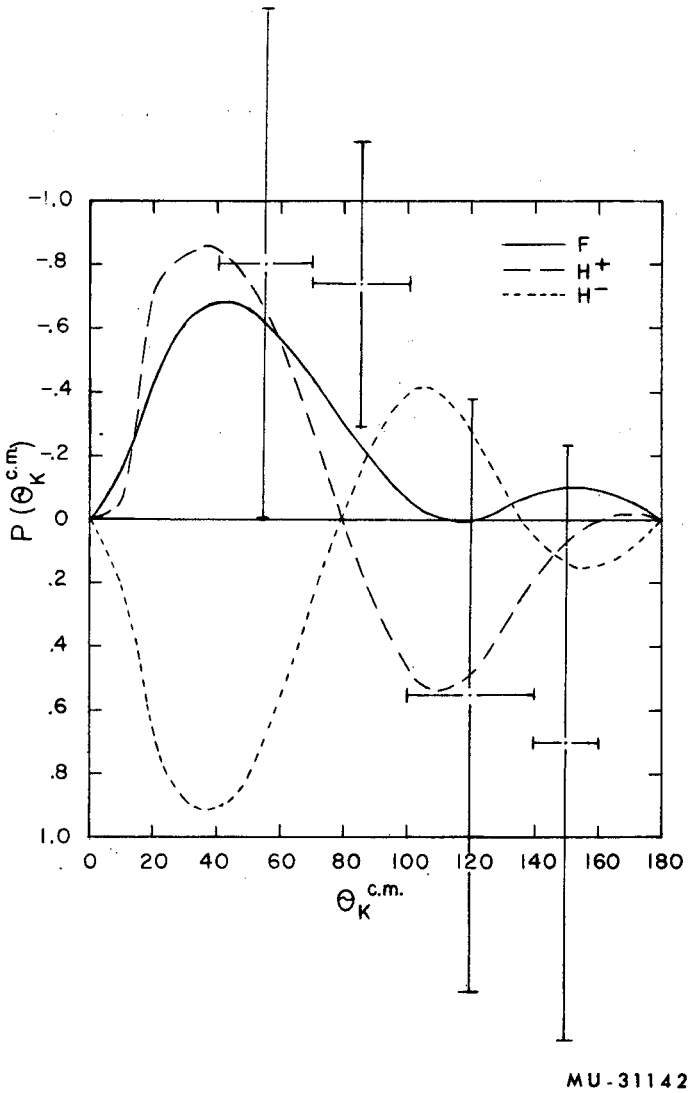

Fig. 5(e). Differential polarization curves [see caption of Fig. 5(a)].

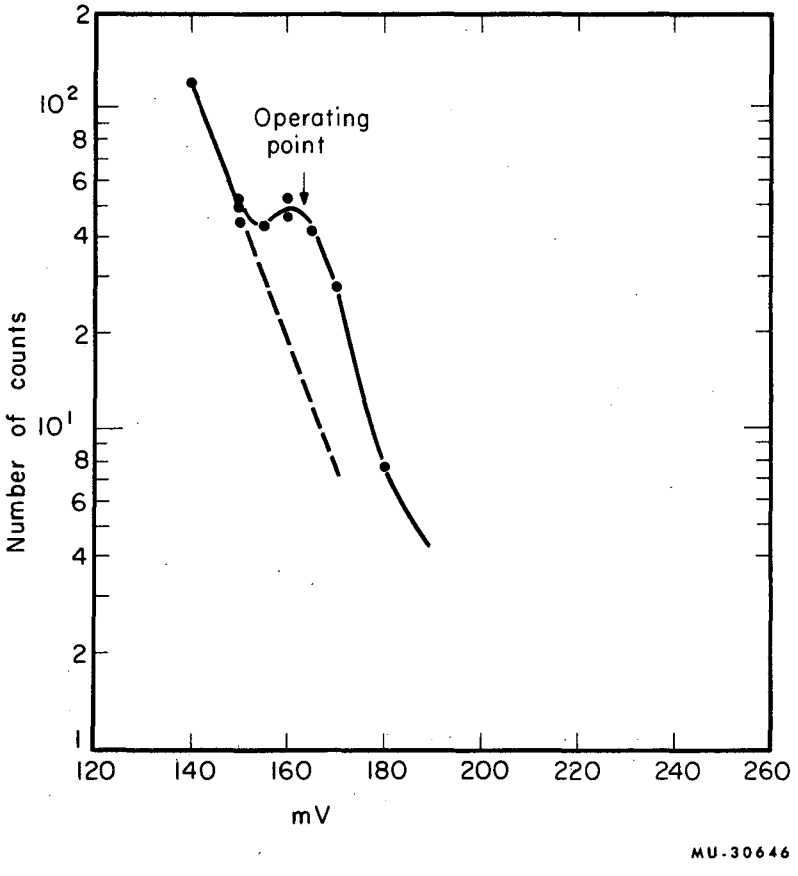

Fig. 6. Typical π-K separation curve at the second slit. The abscissa is in units of shunt voltage for the magnet of one of the spectrometers.

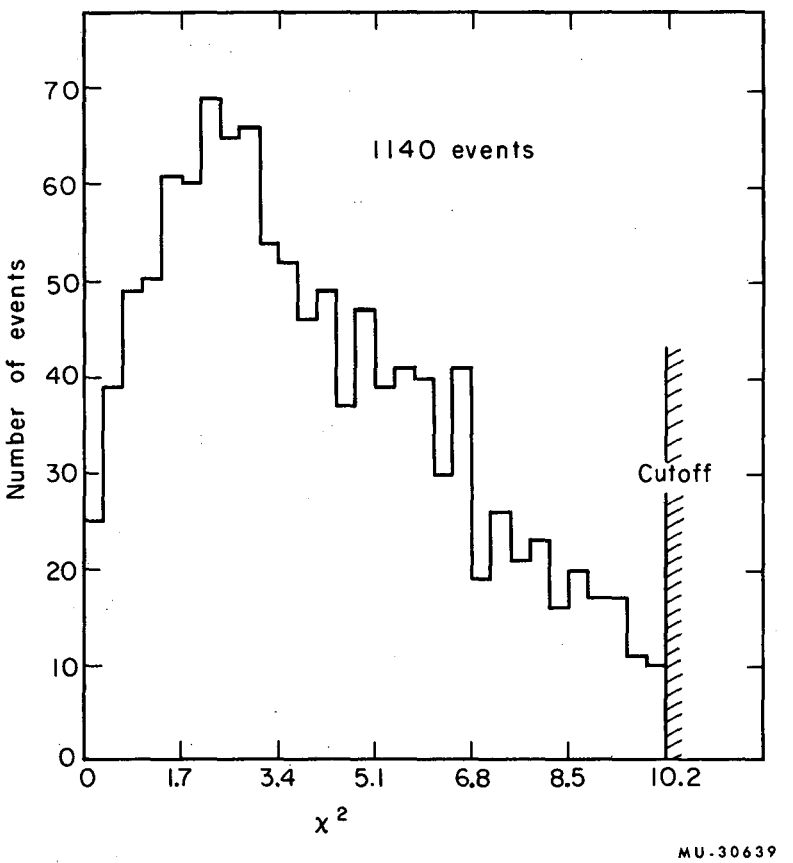

Fig. 7. χ^2 Distribution for K^+-P scatters. The abscissa scale has been adjusted as explained in the text.

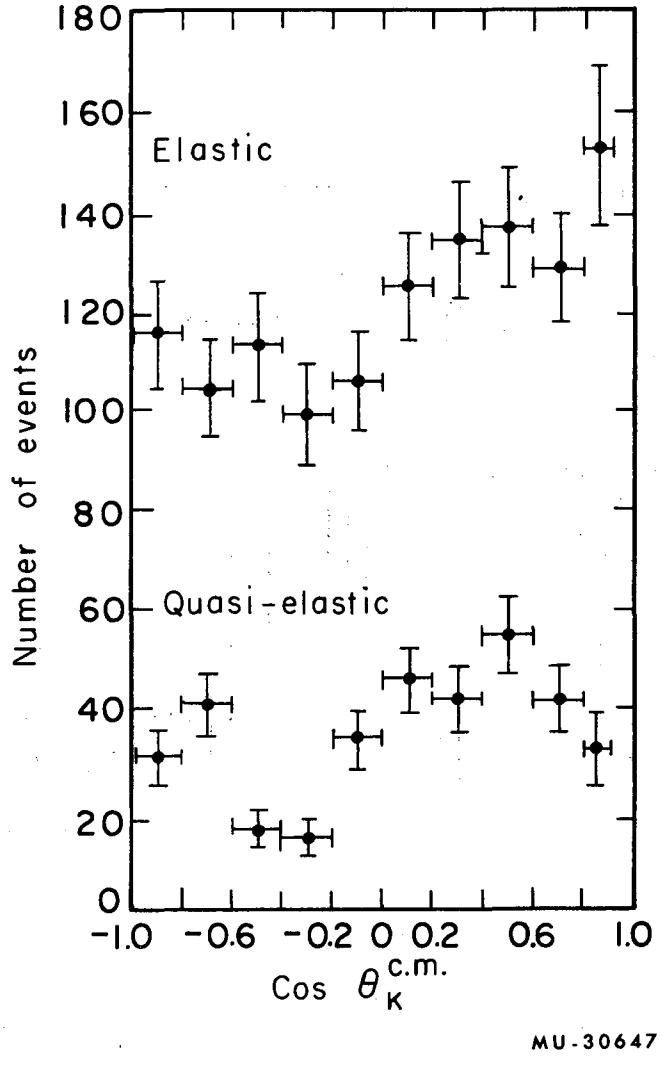

Fig. 8. Comparison of elastic and quasi-elastic scattering. The elastic data is the same as given in Fig. 3.

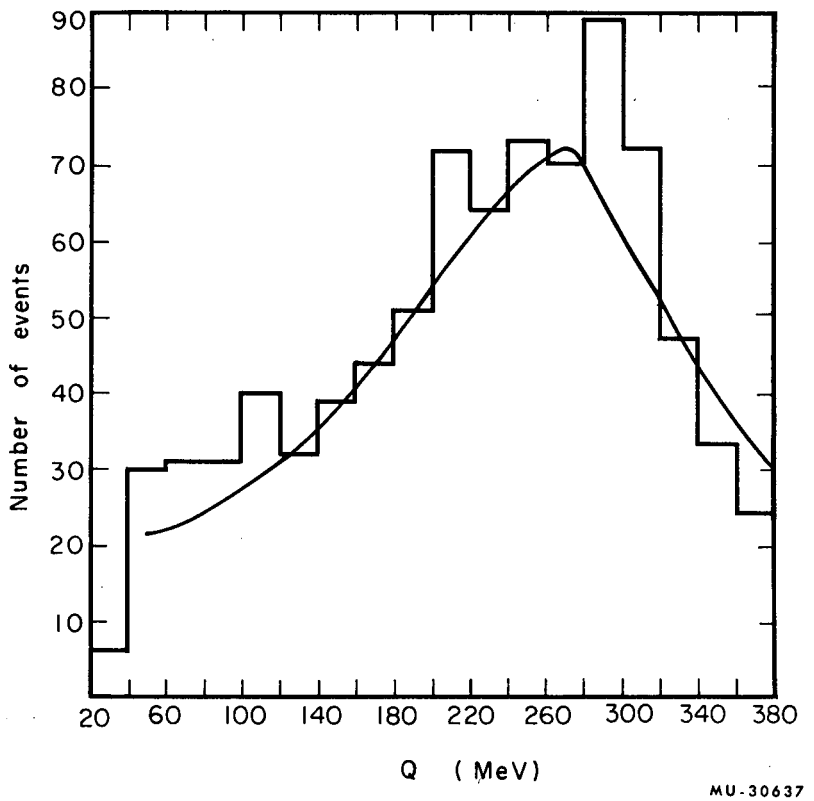

Fig. 9. Q value for inelastic K^+-P events with superimposed carbon phase space curve.

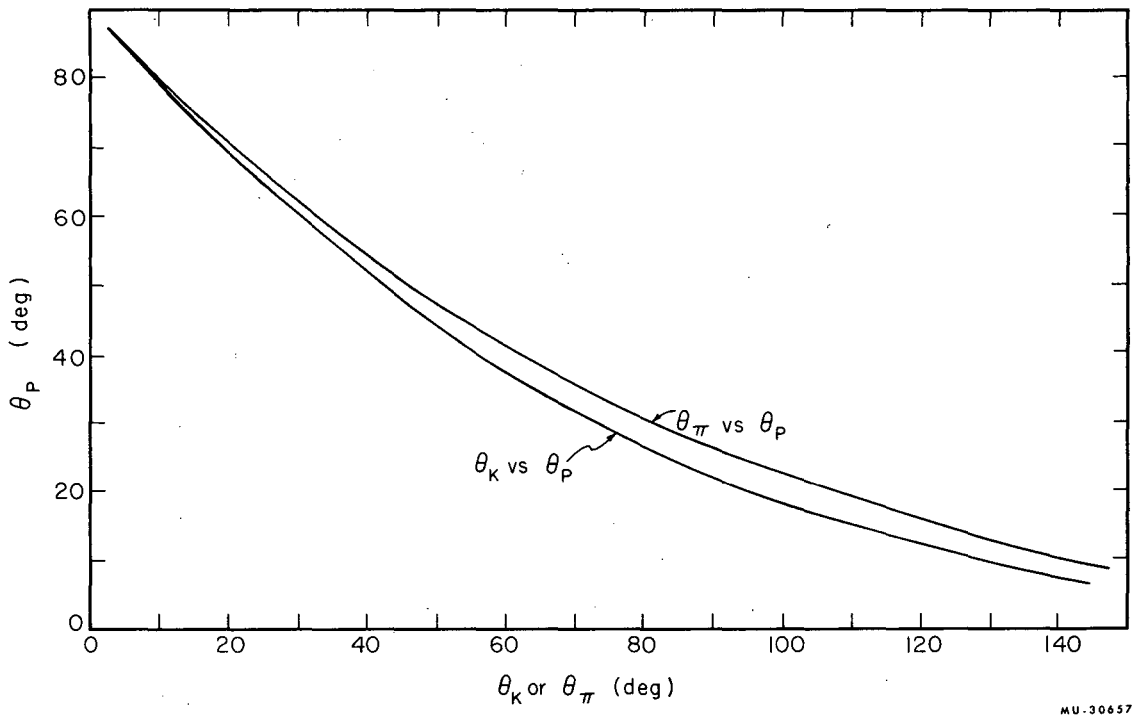

Fig. 10(a). Theoretical curves of laboratory scattering angles.

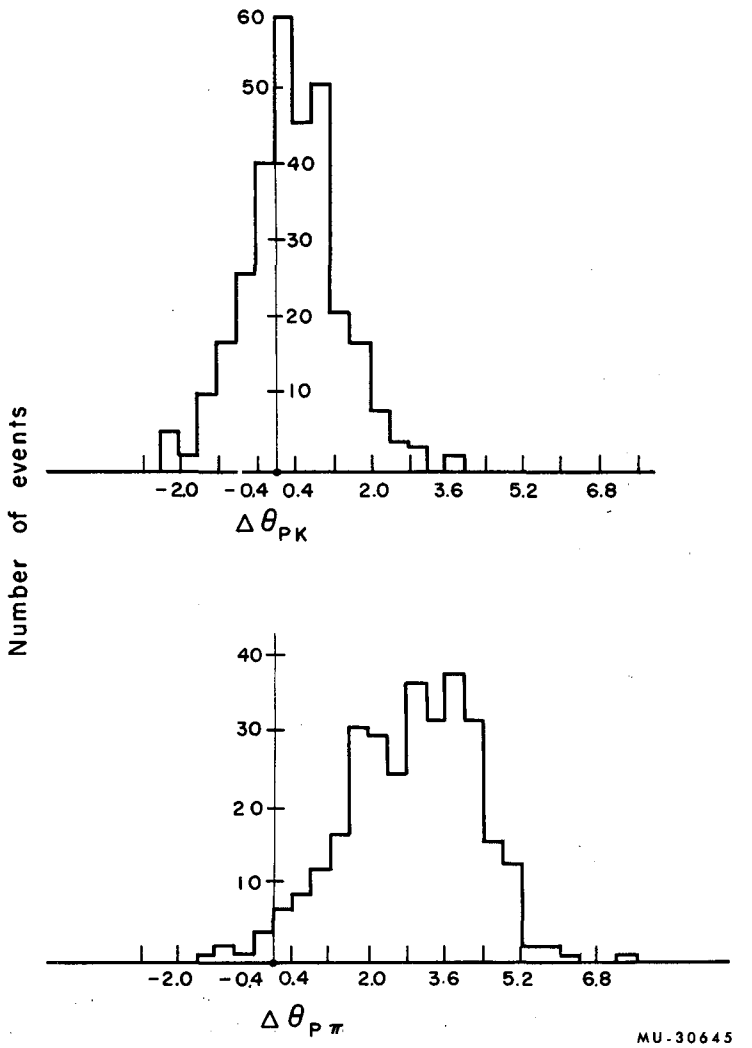

Fig. 10(b) and (c). Perpendicular distance—in degrees—from
(b) the θ_K vs θ_P theoretical curve
(c) the θ_π vs θ_P theoretical curve.

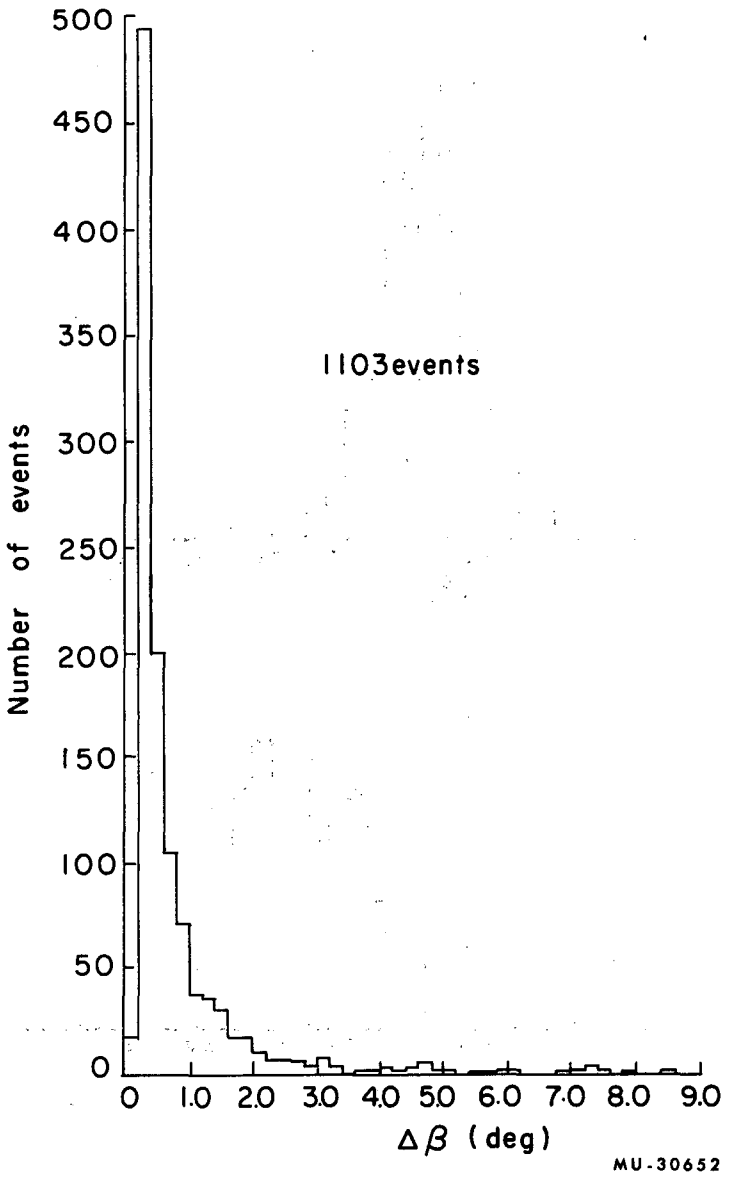

Fig. 11(a). Measurement error in the azimuthal angle for recoil protons at the first scatter. This angle lies in the horizontal (x, y) plane of the bubble chamber.

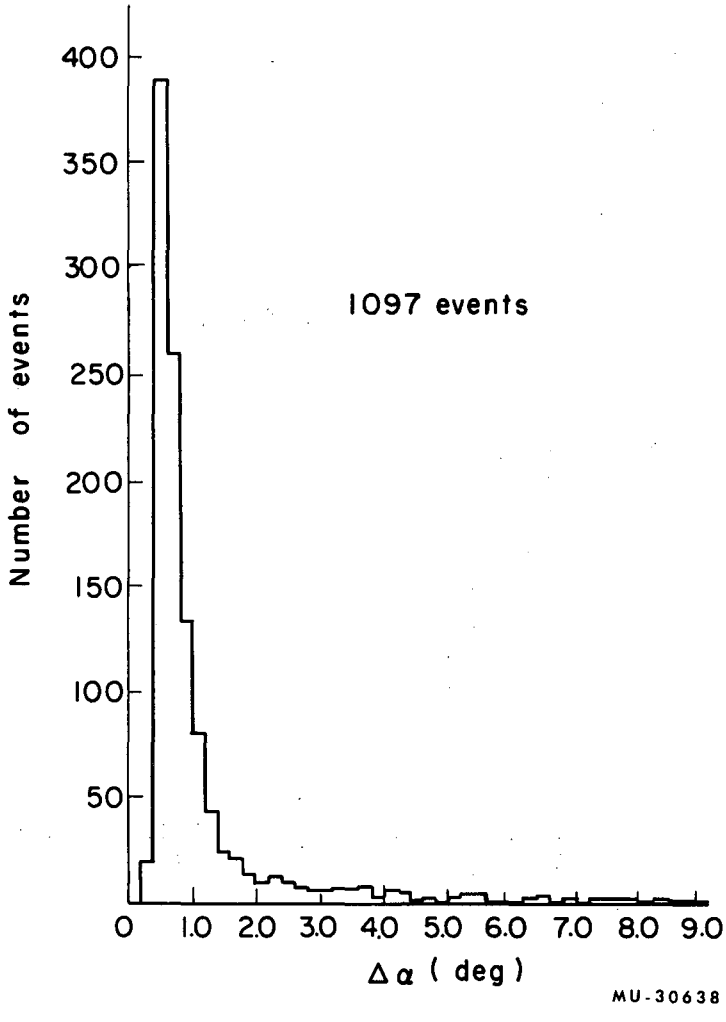

Fig. 11(b). Measurement error in the dip angle for recoil protons at the first scatter. This angle is measured from the vertical ($\hat{z}$) chamber axis.

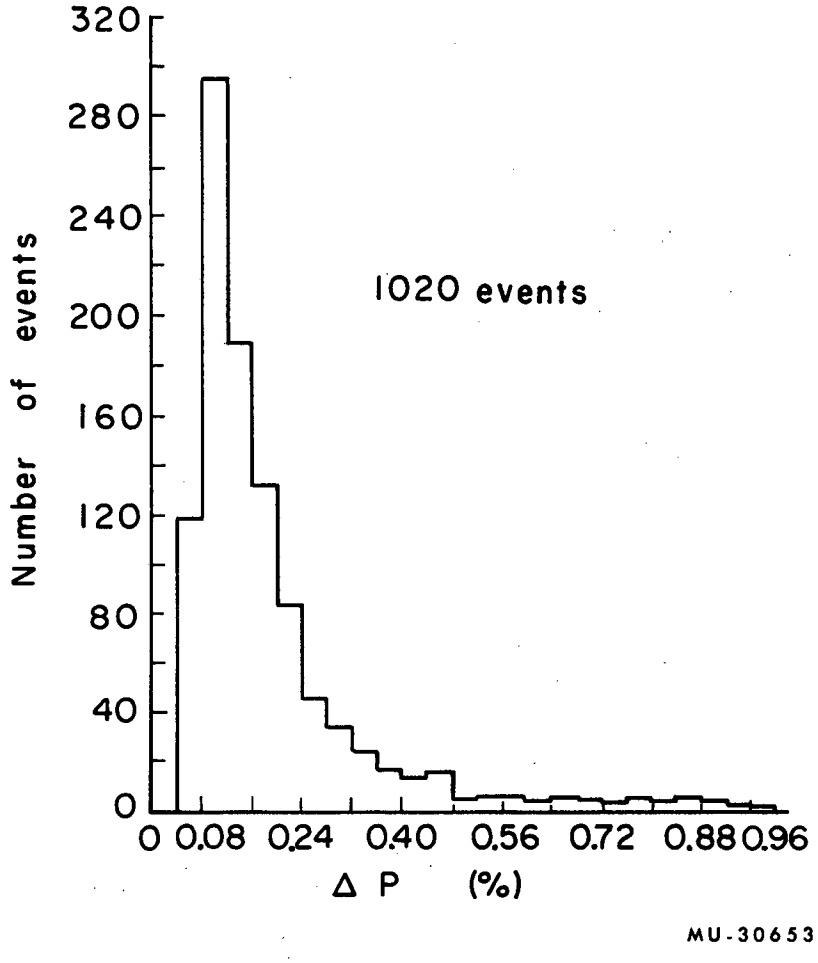

Fig. 11(c). Measurement error in the momentum for recoil protons at the first scatter.

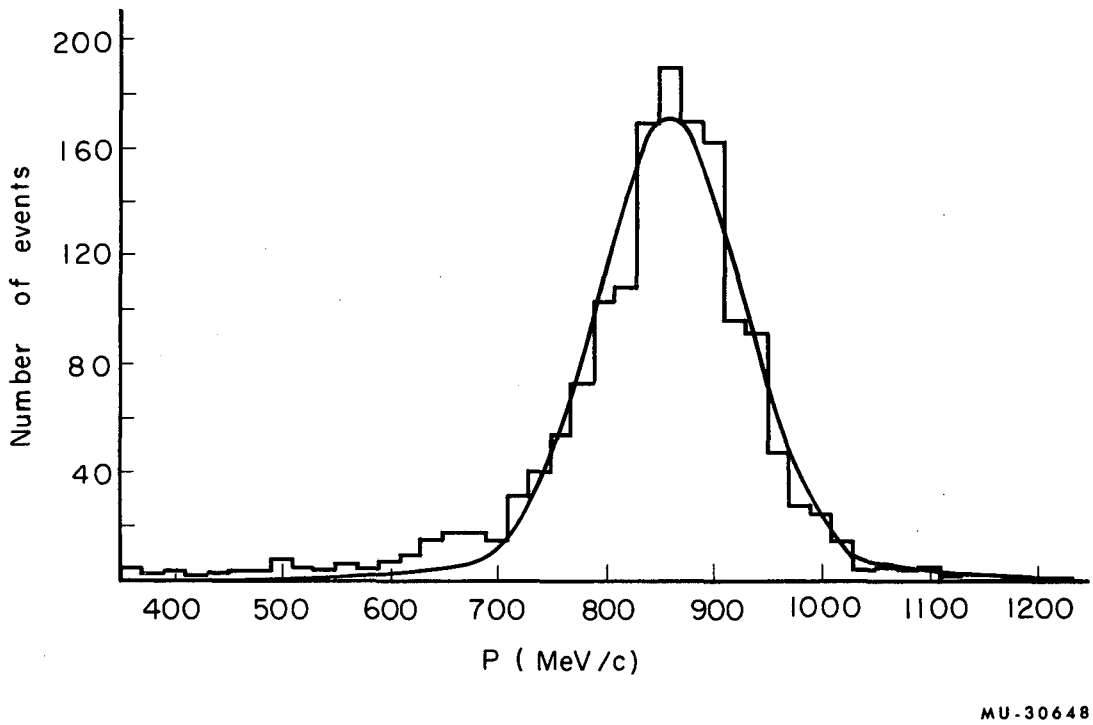

Fig. 12. K^+ beam momentum with fitted Gaussian curve.

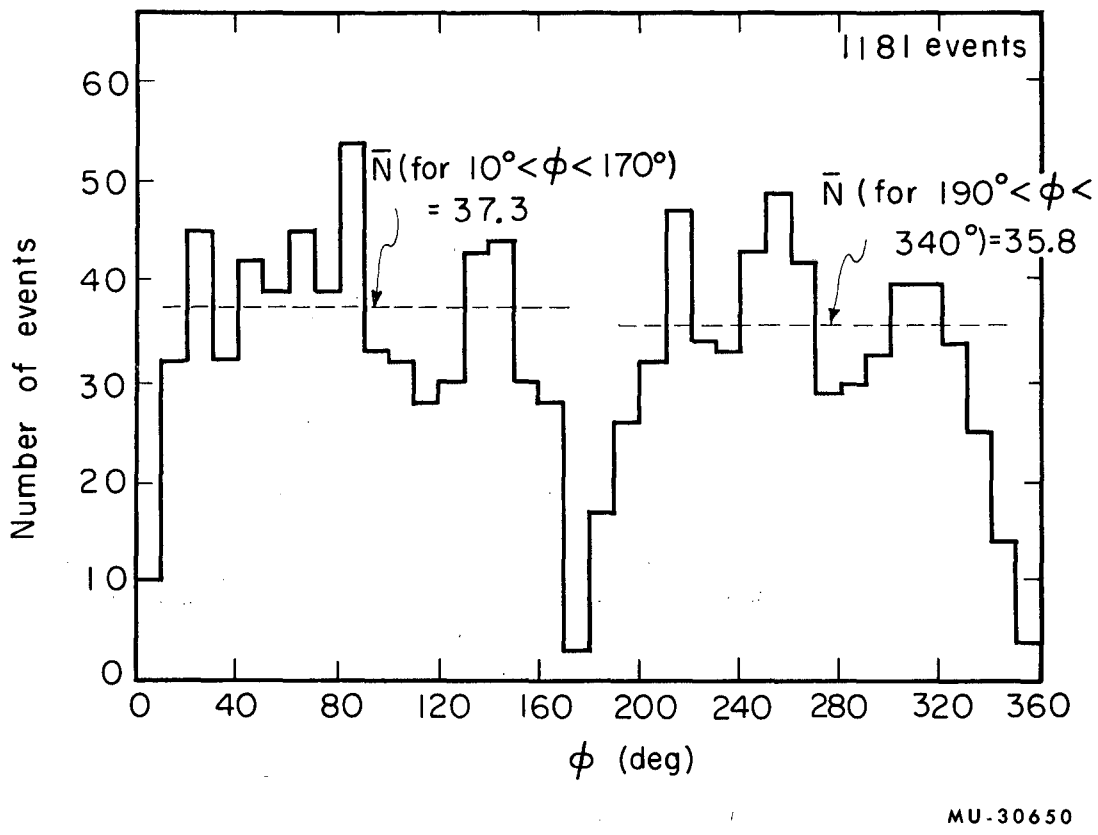

Fig. 13. Azimuthal angle of the scattered K^+ at the first vertex. This angle is measured about the direction of the incident K^+. $\bar{N}$ denotes an average number of events per box in the stated angular region.

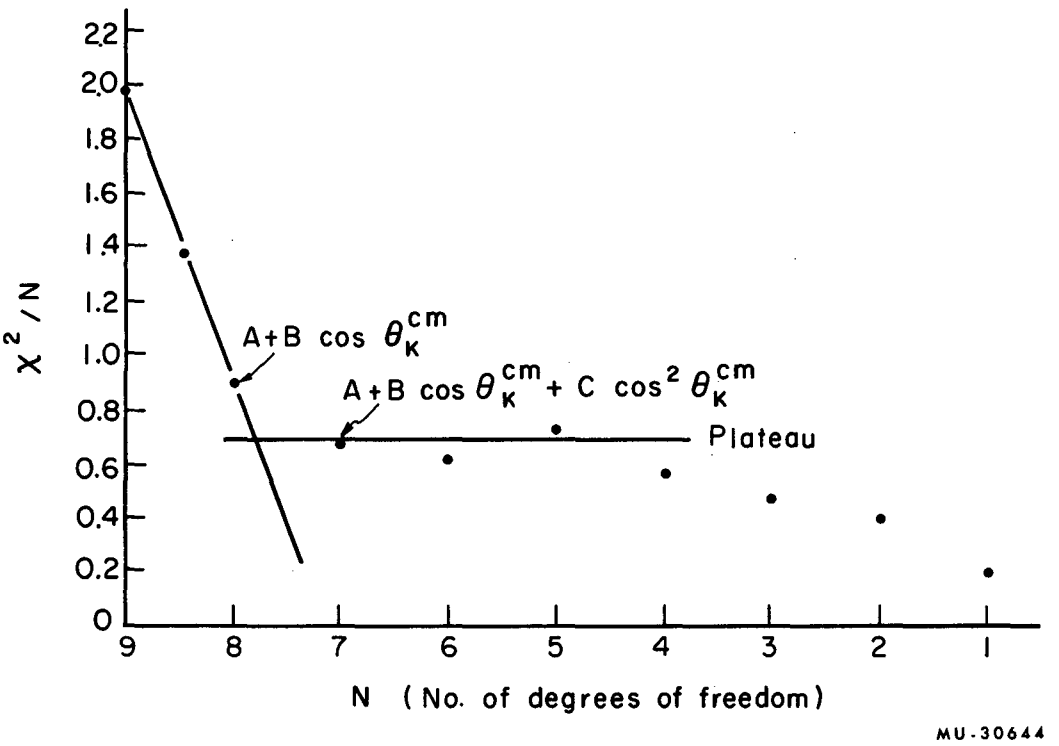

Fig. 14. $\frac{\chi^2}{N}$ vs N, in the cosine series fitting of the angular distribution.

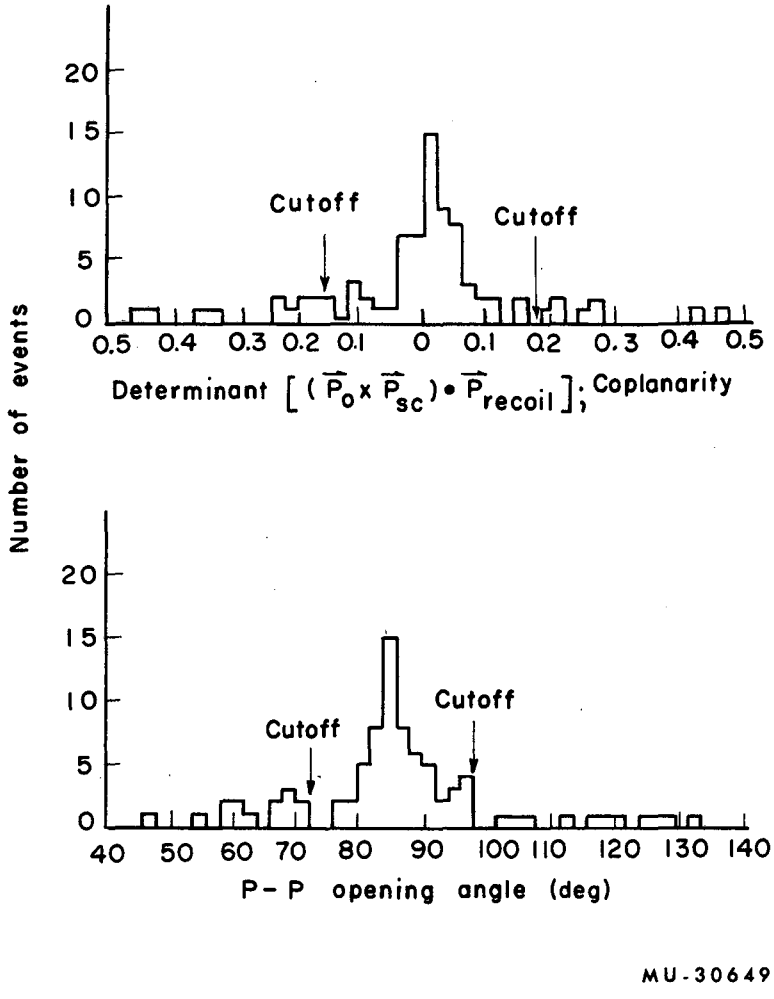

Fig. 15(a). Coplanarity test of P-P scatters.
(b). Opening angle between the scattered protons to test for P-P scatters.

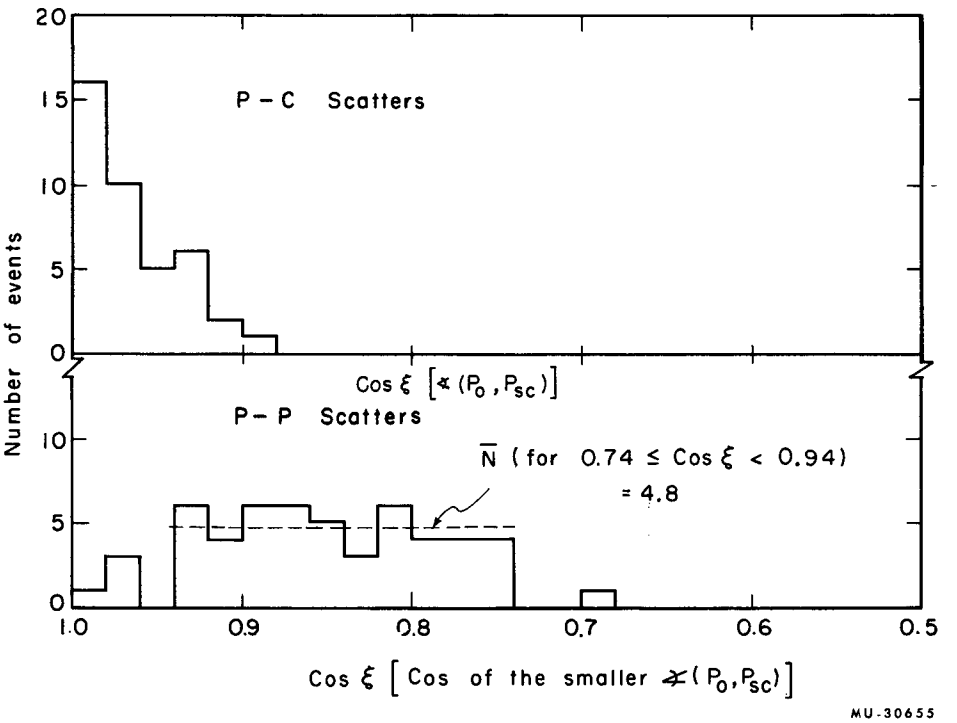

Fig. 16(a). Angular distribution of the scattered proton in P-C interactions.

(b). Angular distribution of the proton in the forward center of mass hemisphere for P-P scatters.

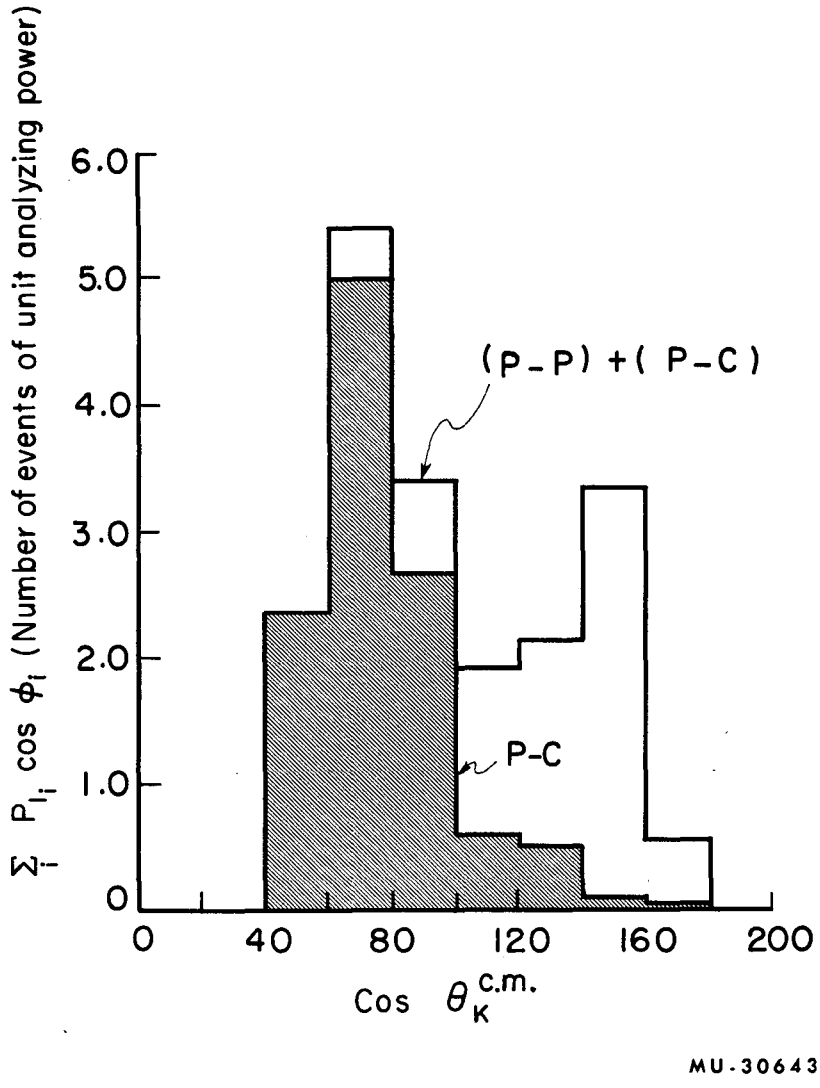

Fig. 17. Angular distribution of the K^+ for events used in the polarization determination; the ordinate is in units of analyzing power, as described in the text.

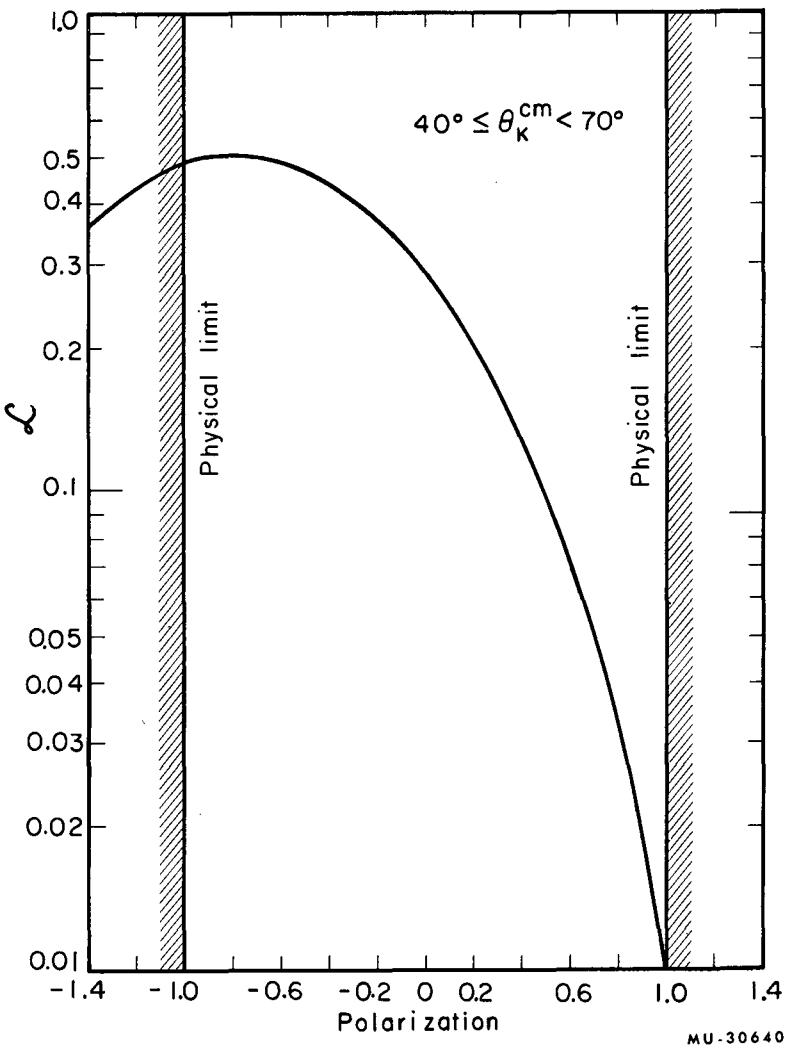

Fig. 18(a). The logarithm of the likelihood function, $\mathcal{L}(P_0)$ vs P_0 over the indicated angular region.

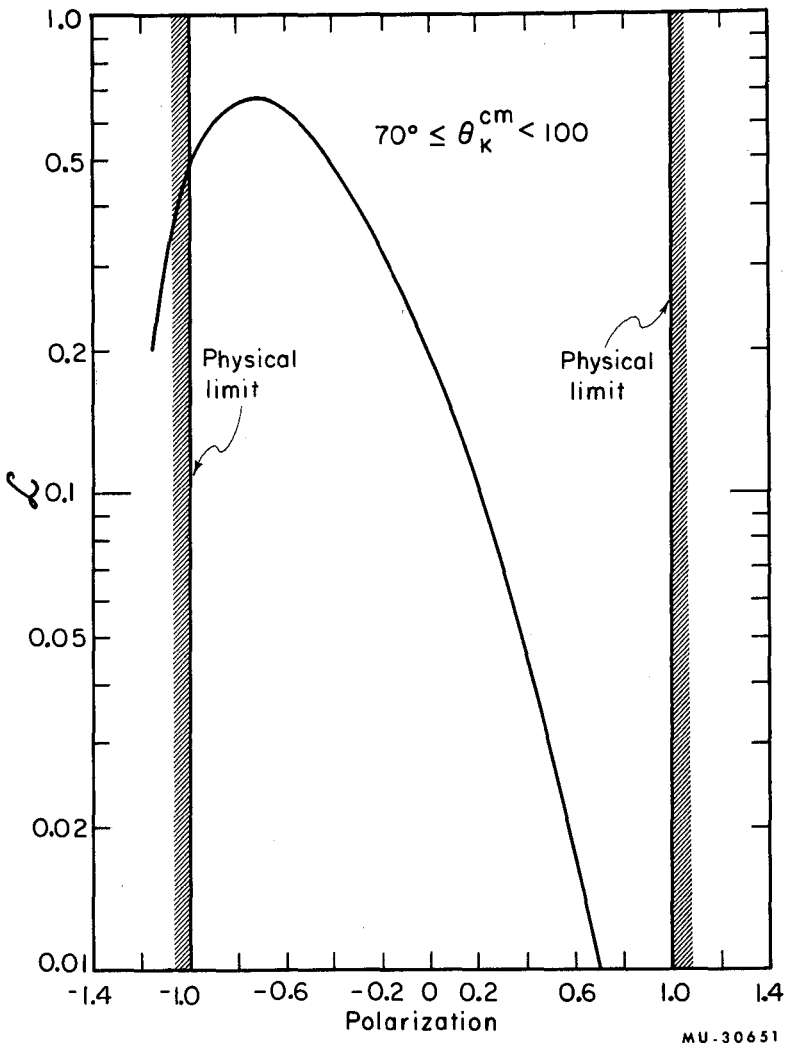

Fig. 18(b). The logarithm of the likelihood function, $\mathcal{L}(P_0)$ vs P_0 in the indicated angular region.

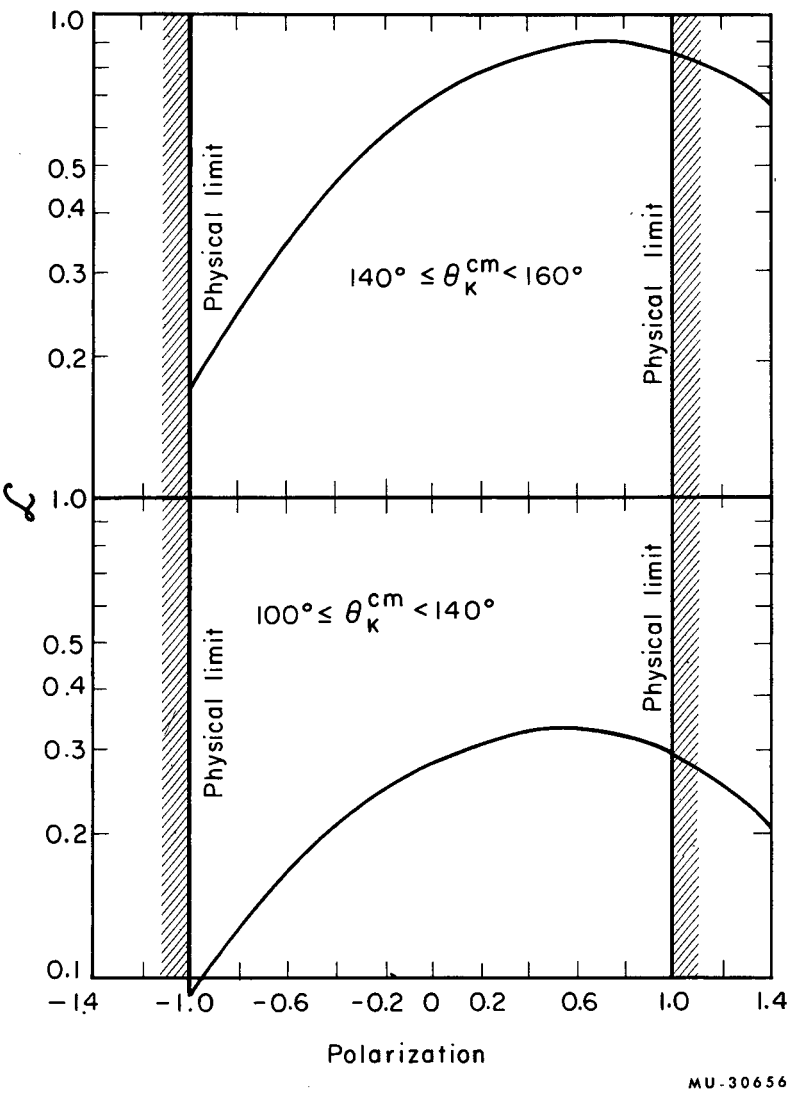

Fig. 18(c) and (d). The logarithm of the likelihood function, $\mathcal{L}(P_0)$, vs P_0 in the indicated angular region.

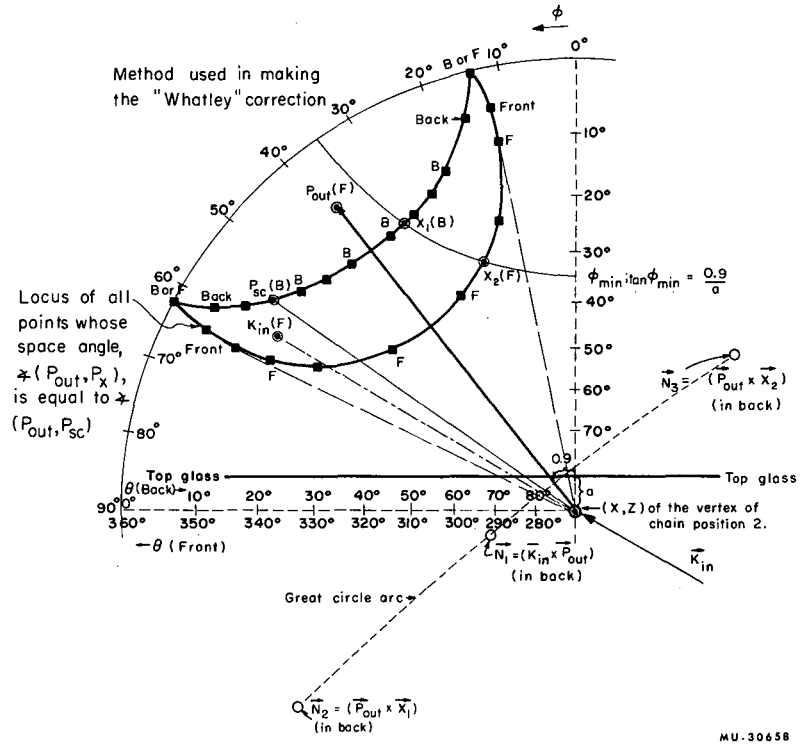

Fig. 19. Procedure for the Whatley correction.

SEP 24 1963